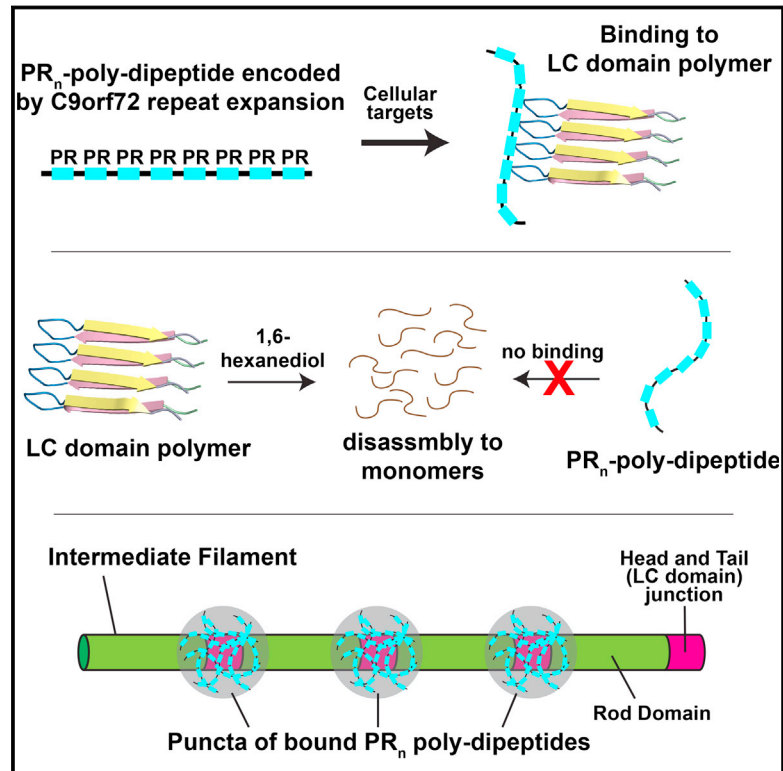


# Toxic PR Poly-Dipeptides Encoded by the C9orf72 Repeat Expansion Target LC Domain Polymers

## Graphical Abstract



## Authors

Yi Lin, Eiichiro Mori, Masato Kato, Siheng Xiang, Leeju Wu, Ilmin Kwon, Steven L. McKnight

## Correspondence

ilmin.kwon@skku.edu (I.K.),  
steven.mcknight@utsouthwestern.edu (S.L.M.)

## In Brief

Toxic proline-arginine poly-dipeptides, which are encoded by C9orf72 hexanucleotide expansions frequently found in amyotrophic lateral sclerosis, bind to polymers of low complexity domain proteins.

## Highlights

- The toxic, C9orf72-encoded PR<sub>n</sub> poly-dipeptide binds many intracellular targets
- The toxic PR<sub>n</sub> poly-dipeptide binds polymeric forms of low complexity sequences
- Aliphatic alcohols melt both low complexity polymers and intracellular puncta
- RNA granules may bind intermediate filaments for proper localization within cells



# Toxic PR Poly-Dipeptides Encoded by the C9orf72 Repeat Expansion Target LC Domain Polymers

Yi Lin,<sup>1,3</sup> Eiichiro Mori,<sup>1,3</sup> Masato Kato,<sup>1,3</sup> Siheng Xiang,<sup>1,3</sup> Leeju Wu,<sup>1</sup> Ilimin Kwon,<sup>2,\*</sup> and Steven L. McKnight<sup>1,4,\*</sup>

<sup>1</sup>Department of Biochemistry, UT Southwestern Medical Center, 5323 Harry Hines Boulevard, Dallas, TX 75390-9152, USA

<sup>2</sup>Department of Anatomy and Cell Biology Sungkyunkwan University School of Medicine, Samsung Biomedical Research Institute, Suwon 16419, Korea

<sup>3</sup>Co-first author

<sup>4</sup>Lead Correspondence

\*Correspondence: [ilimin.kwon@skku.edu](mailto:ilimin.kwon@skku.edu) (I.K.), [steven.mcknight@utsouthwestern.edu](mailto:steven.mcknight@utsouthwestern.edu) (S.L.M.)  
<http://dx.doi.org/10.1016/j.cell.2016.10.003>

## SUMMARY

Two complementary approaches were used in search of the intracellular targets of the toxic PR poly-dipeptide encoded by the repeat sequences expanded in the C9orf72 form of amyotrophic lateral sclerosis. The top categories of PR<sub>n</sub>-bound proteins include constituents of non-membrane invested cellular organelles and intermediate filaments. PR<sub>n</sub> targets are enriched for the inclusion of low complexity (LC) sequences. Evidence is presented indicating that LC sequences represent the direct target of PR<sub>n</sub> binding and that interaction between the PR<sub>n</sub> poly-dipeptide and LC domains is polymer-dependent. These studies indicate that PR<sub>n</sub>-mediated toxicity may result from broad impediments to the dynamics of cell structure and information flow from gene to message to protein.

## INTRODUCTION

The most prevalent form of familial amyotrophic lateral sclerosis (ALS) involves expansion of the GGGGCC (G<sub>4</sub>C<sub>2</sub>) hexanucleotide repeat located within the first intron of a gene designated C9orf72 (DeJesus-Hernandez et al., 2011; Renton et al., 2011). Unaffected individuals contain a modest number of the G<sub>4</sub>C<sub>2</sub> repeats. Affected patients exhibit expansions to upward of 1,000 or more of the repeats. Various concepts have emerged concerning the molecular basis of disease pathophysiology, including impediments to expression of the C9orf72 gene itself (van Blitterswijk et al., 2015), expression of putatively toxic sense or anti-sense transcripts of the repeats (Donnelly et al., 2013; Haeusler et al., 2014; Lagier-Tourenne et al., 2013; Mizielinska et al., 2013), and expression of putatively toxic repeat-associated, non-ATG (RAN) translation products (Ash et al., 2013; Mori et al., 2013; Zu et al., 2013).

Among the five poly-dipeptides encoded by the sense and anti-sense transcripts of the expanded repeat (GA<sub>n</sub>, GP<sub>n</sub>, GR<sub>n</sub>, PA<sub>n</sub> and PR<sub>n</sub>), two display significant toxicity—GR<sub>n</sub> and PR<sub>n</sub>

(Kwon et al., 2014; Mizielinska et al., 2014). Recent studies indicate that the GR<sub>n</sub> and PR<sub>n</sub> poly-dipeptides impede nucleo:cytosolic transport, pre-mRNA splicing, and rRNA biogenesis (Freibaum et al., 2015; Jovičić et al., 2015; Kwon et al., 2014; Wen et al., 2014).

Missing to date are unbiased studies of the direct intracellular targets of GR<sub>n</sub> and PR<sub>n</sub> that may explain the toxicity of these poly-dipeptides. Here, we have used two complementary approaches to identify proteins bound by the PR<sub>n</sub> poly-dipeptide. Evidence is presented indicating binding of PR<sub>n</sub> to numerous proteins associated with nuclear and cytoplasmic puncta not surrounded by investing membranes, as well as nucleoli, nuclear pores, and intermediate filaments. Concordant data from Taylor and colleagues report a distribution of 514 PR<sub>n</sub> and GR<sub>n</sub> interacting proteins (Lee et al., 2016, this issue), the identities of which overlap significantly with the PR<sub>n</sub> targets identified herein. These independent studies indicate that PR<sub>n</sub> toxicity may result from widespread impediments to cell organization and function.

Common among PR<sub>n</sub> target proteins are low complexity (LC) domains shown herein to be both necessary and sufficient for PR<sub>n</sub> binding. In previous studies we have found that LC domains can polymerize into amyloid-like fibers (Kato et al., 2012; Han et al., 2012). A key feature of LC-domain polymers is their lability to de-polymerization. Here, we have employed several independent assays giving evidence that PR<sub>n</sub> binding to its targets require that LC domains exist in a cross-β polymeric state.

Most surprising among newly discovered targets of the toxic PR<sub>n</sub> poly-dipeptide are intermediate filament proteins. The PR<sub>n</sub> poly-dipeptide binds to polymeric forms of the LC domains located at the amino terminal ends of intermediate filament proteins. These and other data favor the possibility of direct interaction between RNA granules and intermediate filaments. Such observations may offer mechanistic insight into the manner in which RNA granules segregate to spatially restricted regions within eggs, embryos, or individual cells.

## RESULTS

A synthetic peptide consisting of 20 repeats of the PR<sub>n</sub> poly-dipeptide was modified to contain a benzophenone for photo-crosslinking, an alkyne moiety for the use of click chemistry,



excised from the gel and identified by shotgun mass spectrometry (Table S2). The top categories of the 177 PR<sub>100</sub>-bound proteins included RNA binding proteins, intermediate filament proteins, and DEAD box RNA helicase enzymes. The Venn diagram shown in Figure 1C compares proteins identified by both approaches. 72% of the 177 proteins co-precipitated with the 3xFlag:PR<sub>100</sub> probe were also cross-linked to the PR<sub>20</sub>BAH probe (Table S3). The statistical probability of this level of overlap is exceedingly low ( $p = 7.2 \times 10^{-103}$ ).

### The PR<sub>n</sub> Poly-Dipeptide Preferentially Interacts with LC Domains

Both categories of PR<sub>n</sub>-bound proteins were enriched for the inclusion of proteins containing low complexity (LC) domains. By use of a straightforward algorithm (SEG program) (Wootton, 1994), the lists of proteins either cross-linked or co-precipitated by the PR<sub>n</sub> probes were inspected for species containing an LC domain of 50 or more amino acids. This algorithm can be deployed using amino acid windows variable in size. The 50 amino acid window we have employed is relatively stringent for the identification of LC domains and follows the recommendations articulated by others (Dyson and Wright, 2005). Compared with the human proteome, wherein LC domains are found in 10.3% of all proteins, 15.1% of PR<sub>20</sub>BAH cross-linked proteins contained LC domains, and 20.9% of 3xFlag:PR<sub>100</sub>-bound proteins contained LC domains. Of the 120 proteins found in both lists (Table S3), 21.7% contained LC domains. In summary, irrespective of method used, the PR<sub>n</sub> poly-dipeptide was found to interact preferentially with LC domain-containing proteins (Figure 1C).

To more directly investigate polypeptide domains required for PR<sub>n</sub> interaction, three GFP:hnRNPA1 fusion proteins were prepared. One fusion protein linked GFP to the full-length hnRNPA1 protein, another linked GFP to the two RRM domains of hnRNPA1, and a third linked GFP to the C-terminal LC domain of hnRNPA1. Each fusion protein was expressed in bacteria, purified, and incubated with a synthetic peptide consisting of 20 PR dipeptide repeats linked to an HA epitope tag (PR<sub>20</sub>HA). Following incubation, the samples were immunoprecipitated with beads linked to antibodies to the HA epitope, eluted, electrophoresed on a denaturing SDS-PAGE gel, and visualized by Coomassie blue staining (Figure 1D). Clear evidence of PR<sub>20</sub>HA-mediated precipitation was observed for the GFP variant fused to either the intact hnRNPA1 polypeptide or the variant containing only the LC domain of hnRNPA1. By contrast, no precipitation was observed for the GFP fusion containing only the two, N-terminal RRM domains. These observations provide evidence for both the necessity and sufficiency of the LC domain of hnRNPA1 for interaction with the synthetic PR<sub>20</sub>HA poly-dipeptide.

### Hierarchical Melting of LC Domain Polymers and Liquid-Like Droplets by Aliphatic Alcohols

When incubated at neutral pH and physiologic ionic strength, the LC domains of numerous RNA binding proteins polymerize into labile, cross- $\beta$  fibers. It has been hypothesized that these amyloid-like polymers may help organize intracellular structures not surrounded by investing membranes (Han et al., 2012; Kato

et al., 2012). Knowing that targets of the toxic PR<sub>n</sub> poly-dipeptide are enriched for the inclusion of LC domains (Figures 1A–1C), and that LC domains are both necessary and sufficient for PR<sub>n</sub> binding (Figure 1D), the question arises as to whether PR<sub>n</sub> binding might require LC domains to exist in a cross- $\beta$  polymeric state?

Obvious utility might be found in the form of chemical agents capable of correlatively affecting labile cross- $\beta$  polymers and intracellular puncta enriched in LC-bearing proteins. Aliphatic alcohols, including 1,6-hexanediol (1,6-HD), are known to melt nucleopores, RNA granules, polar granules, and certain other nuclear and cytoplasmic puncta not bound by investing membranes (Kroschwald et al., 2015; Patel et al., 2007; Updike et al., 2011). Knowing that these intracellular puncta are enriched in both PR<sub>n</sub> targets and LC sequences, we investigated the effects of four related aliphatic alcohols on LC domain polymers.

In order to study the effects of aliphatic alcohols on labile, amyloid-like polymers formed from LC domains, we exposed mCherry:FUS hydrogel droplets to a series of aliphatic alcohols including 1,6-HD, 2,5-hexanediol (2,5-HD), 1,5-pentanediol (1,5-PD) and 1,4-butanediol (1,4-BD). As shown in Figure 2A, and the video accessible from Movie S1, mCherry:FUS hydrogel droplets were melted by 1,6-HD largely to the exclusion of the other three aliphatic alcohols. 1,5-PD required overnight incubation to melt mCherry:FUS hydrogel droplets, and no hydrogel melting was observed for either 2,5-HD or 1,4-BD.

More quantitative assessment of polymer disassembly was conducted using light scattering assays. Fibrous, pre-gelation preparations of mCherry:FUS were monitored by light scattering as a function of exposure to the four aliphatic alcohols listed above. 1,6-HD attenuated light scattering in a concentration-dependent manner. mCherry:FUS polymers dissolved partially in a time-dependent manner when exposed to 5% 1,6-HD. More prominent melting was observed at 10% and 15% levels of 1,6-HD (Figure S2). Among the four aliphatic alcohols, little or no diminution in light scattering was observed for 2,5-HD or 1,4-BD (Figure 2B). Fiber melting was observed when mCherry:FUS polymers were exposed to 15% 1,5-PD, but to a lesser extent than the same concentration of 1,6-HD. In contrast to its ability to melt labile cross- $\beta$  polymers formed from LC domains, 1,6-HD failed to affect the polymeric state of A $\beta$  amyloid fibers (Figure 2C).

The LC domains of RNA binding proteins participate in the formation of liquid-like droplets (Lin et al., 2015; Molliex et al., 2015; Patel et al., 2015). This phenomenon of phase separation is believed to be reflective of the chemical forces involved in formation of intracellular puncta including RNA granules. Various lines of evidence have supported the hypothesis that cross- $\beta$  polymerization of LC domains may participate in the formation of liquid-like droplets (Xiang et al., 2015).

Two types of liquid-like droplets were used to test the effects of aliphatic alcohols on phase-separated protein samples. A fusion protein containing maltose binding protein (MBP) linked to the RNA binding domain of poly-pyrimidine track binding protein (PTB) and the LC sequence of hnRNPA2 was treated with TEV protease to remove the solubilizing MBP and simultaneously exposed to a synthetic RNA containing five PTB binding

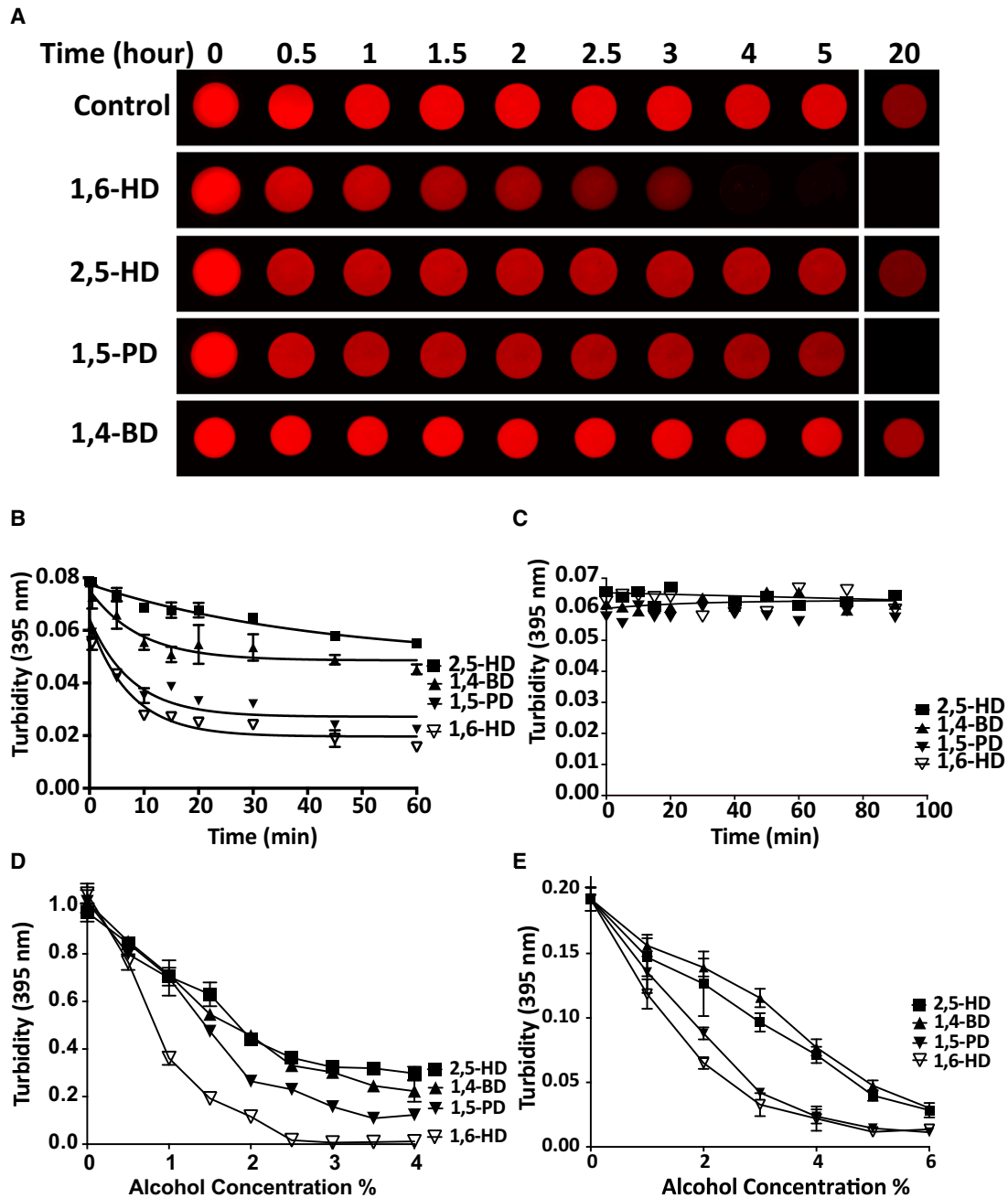


**Figure 2. Melting of Hydrogels, LC Domain Polymers, and Liquid-Like Droplets by Aliphatic Alcohols**

(A) mCherry:FUS hydrogel droplets were incubated with 15% levels of indicated aliphatic alcohols for varying intervals from 30 min to 20 hr (See also [Movie S1](#)). (B) Melting of mCherry:FUS polymers in suspension with 15% of indicated aliphatic alcohols as measured by light scattering at 395 nm ( $n = 3$ , data are presented as means  $\pm$  SD. Note that error bars for most of the data points are smaller than the symbols. See also [Figure S2](#)). (C) Exposure of A $\beta$  amyloid fibers to 15% levels of indicated aliphatic alcohols. No change in turbidity (395nm) was observed for up to 90 min. (D) Liquid-like droplets were formed by mixing an MBP:PTB:hnRNPA2 triple fusion protein with TEV protease and a synthetic RNA substrate ([STAR Methods](#)), followed by exposure to 0.5%–4% levels of the indicated aliphatic alcohols ( $n = 2$ , data are presented as means  $\pm$  SD). (E) FUS liquid-like droplets were exposed to 0.5%–6% levels of the indicated aliphatic alcohols ( $n = 2$ , data are presented as means  $\pm$  SD).

sites ([STAR Methods](#)). Liquid-like droplets began to appear within minutes after TEV protease cleavage and could be detected spectrophotometrically by light scattering or visualized by light microscopy. Samples of liquid-like droplets were

exposed to four aliphatic alcohols at concentrations ranging from 0.5%–4%. As shown in [Figure 2D](#), liquid-like droplets were melted most substantially by 1,6-HD, less so by 1,5-PD, and least by 2,5-HD or 1,4-BD.

A similar pattern of effects was observed when the same four aliphatic alcohols were applied to liquid-like droplets formed by the LC domain of FUS. The LC domain of FUS became phase-separated into liquid-like droplets upon dilution of concentrated, urea solubilized protein into urea-free aqueous buffer (STAR Methods). Exposure of the FUS droplets to aliphatic alcohols resulted in melting as deduced by either light microscopy or light scattering. The rank order of droplet melting activity by the four aliphatic alcohols—1,6-HD > 1,5-PD > 2,5-HD = 1,4-BD—was the same for FUS liquid-like droplets as for melting of mCherry:FUS hydrogels (Figure 2A), mCherry:FUS pre-gelation polymers (Figure 2B), and hnRNPA2 liquid-like droplets (Figures 2C and 2D).

### Hierarchical Melting of Intracellular Structures by Aliphatic Alcohols

Having observed a rank order of different aliphatic alcohols on the melting of hydrogels, cross- $\beta$  polymers, and liquid-like droplets, we next tested the abilities of the four alcohols to melt various cellular structures. Cytoplasmic stress granules were visualized in cultured HeLa cells with antibodies to the TIA1 RNA binding protein, Cajal bodies were visualized with antibodies to coilin, and nuclear speckles were visualized with antibodies to the SC35 pre-mRNA splicing factor. Before fixation and immunofluorescent visualization of the various puncta, cells were exposed to either vehicle or 6%–8% levels of 1,6-HD, 2,5-HD, 1,5-PD, or 1,4-BD. Stress granules, Cajal bodies, and nuclear speckles were melted in response to 1,6-HD and 1,5-PD, but not 2,5-HD or 1,4-BD (Figure 3A).

Similar studies were extended to visualize the effects of aliphatic alcohols on cytoskeletal structures including actin filaments, microtubules, and intermediate filaments. None of the aliphatic alcohols were observed to perturb actin filaments or microtubules (Figure 3B). By contrast 1,6-HD and 1,5-PD markedly changed the cytoplasmic organization of both keratin and vimentin intermediate filaments. The prototypic network of intermediate filaments rapidly dispersed into hundreds of small puncta following brief exposure to 8% levels of either of the two aliphatic alcohols. No alterations in the intermediate filament networks of either keratin or vimentin were observed in cells treated with either 2,5-HD or 1,4-BD.

### Pharmacologic Evidence of Polymer-Dependent PR<sub>20</sub> Binding to the LC Domain of hnRNPA2

Previous studies have shown that the PR<sub>n</sub> and GR<sub>n</sub> poly-dipeptides encoded by the C9orf72 repeat expansion bind to hydrogels composed of amyloid-like polymers of the LC domains of various RNA binding proteins (Kwon et al., 2014). It has been hypothesized that the iterative nature of the PR<sub>n</sub> poly-dipeptide repeats might engage epitopes repetitively displayed on the surface of LC domain polymers. If so, PR<sub>n</sub> interaction would be expected to be enhanced for polymeric forms of LC domains relative to their unfolded, monomeric state.

To test this idea, polymeric fibers formed from the LC domain of hnRNPA2 were exposed to varying concentrations of either 1,6-HD or 2,5-HD. As deduced by measurements of light scattering, 1,6-HD caused fiber melting between 5% and 7% of added alcohol (Figure 4A). By contrast, only minimal evidence of fiber melting was observed in samples exposed to as much

as 9% 2,5-HD. Post-exposure to either of the two aliphatic alcohols, samples were mixed with the PR<sub>20</sub>HA peptide, immunoprecipitated with antibodies specific to the HA tag present on the PR<sub>20</sub> peptide, and run on denaturing SDS gels. The 20 kDa LC domain of hnRNPA2 was visualized by Coomassie staining. As shown in Figures 4B, incubation of the binding mixtures with 1,6-HD attenuated PR<sub>n</sub>-mediated precipitation of the hnRNPA2 LC domain. Binding began to diminish at 5% of the aliphatic alcohol and was eliminated by the 8% level. Unlike 1,6-HD, 2,5-HD did not diminish PR<sub>20</sub>-mediated precipitation of the LC domain of hnRNPA2 even at the highest alcohol concentration tested (9%).

Having observed 1,6-HD-mediated impediments to the binding of PR<sub>20</sub> to the LC domain of recombinant hnRNPA2, we tested whether aliphatic alcohols might impede binding of the PR<sub>100</sub> poly-dipeptide to its native, intracellular targets. U2OS cells conditionally expressing the 3xFlag:PR<sub>100</sub> protein were induced with doxycycline, frozen, and powdered using cryo-mill technology. Frozen powder was resuspended at 100 mg/ml and rapidly subjected to immunoprecipitation using anti-flag magnetic beads (STAR Methods). Samples were resuspended in the absence of aliphatic alcohols, or in the presence of 6% 1,6-HD. As shown in Figure 4C, the majority of PR<sub>100</sub>-co-precipitated proteins were lost upon exposure of the lysate to the aliphatic alcohol. Western blot assays were used to interrogate the effects of 1,6-HD on the co-precipitation of PR<sub>n</sub> intracellular targets. Significant reductions were effected by 1,6-HD on co-precipitation of the vimentin, FUS, and C1QBP proteins (Figure S3).

### Molecular Genetic Evidence of Polymer-Dependent Binding of PR<sub>20</sub> to the LC Domain of hnRNPA2

Human genetic studies have described mutations in the genes encoding three different hnRNPs that lead to amyotrophic lateral sclerosis (Kim et al., 2013), frontotemporal dementia (Lee et al., 2013), or limb girdle muscular dystrophy (Vieira et al., 2014). Remarkably, the same aspartic acid within the LC domains is mutated, most frequently to valine, in each of the different proteins/diseases. LC domain fibers formed from the mutated variants are more stable than those formed from the LC domains of the wild-type versions of the three proteins. When run on agarose gels in the presence of varying concentrations of SDS, polymeric fibers of each of the native LC domains dissolved upon dilution and migrated as monomers (Figure S4). By contrast, the mutated variants of the LC domains of hnRNPA1, hnRNPA2, and hnRNPD1 all migrated as polymeric aggregates largely unaffected by the addition of SDS.

As tested by immunoprecipitation, the D290V variant of the hnRNPA2 LC domain bound HA-tagged PR<sub>20</sub> as well or better than the native form of the protein (Figure 4D). Phenylalanine-to-serine mutation of the residue (F291) on the immediate, C-terminal side of the aspartic acid commonly mutated in various disease settings severely limits polymerization of the LC domain of hnRNPA2 (Xiang et al., 2015). This polymer-incompetent variant of the LC domain of hnRNPA2 failed to bind the HA-tagged PR<sub>20</sub> peptide (Figure 4D). In summary, either pharmacologic or mutational disruption of LC domain polymers significantly impeded PR<sub>20</sub> binding.

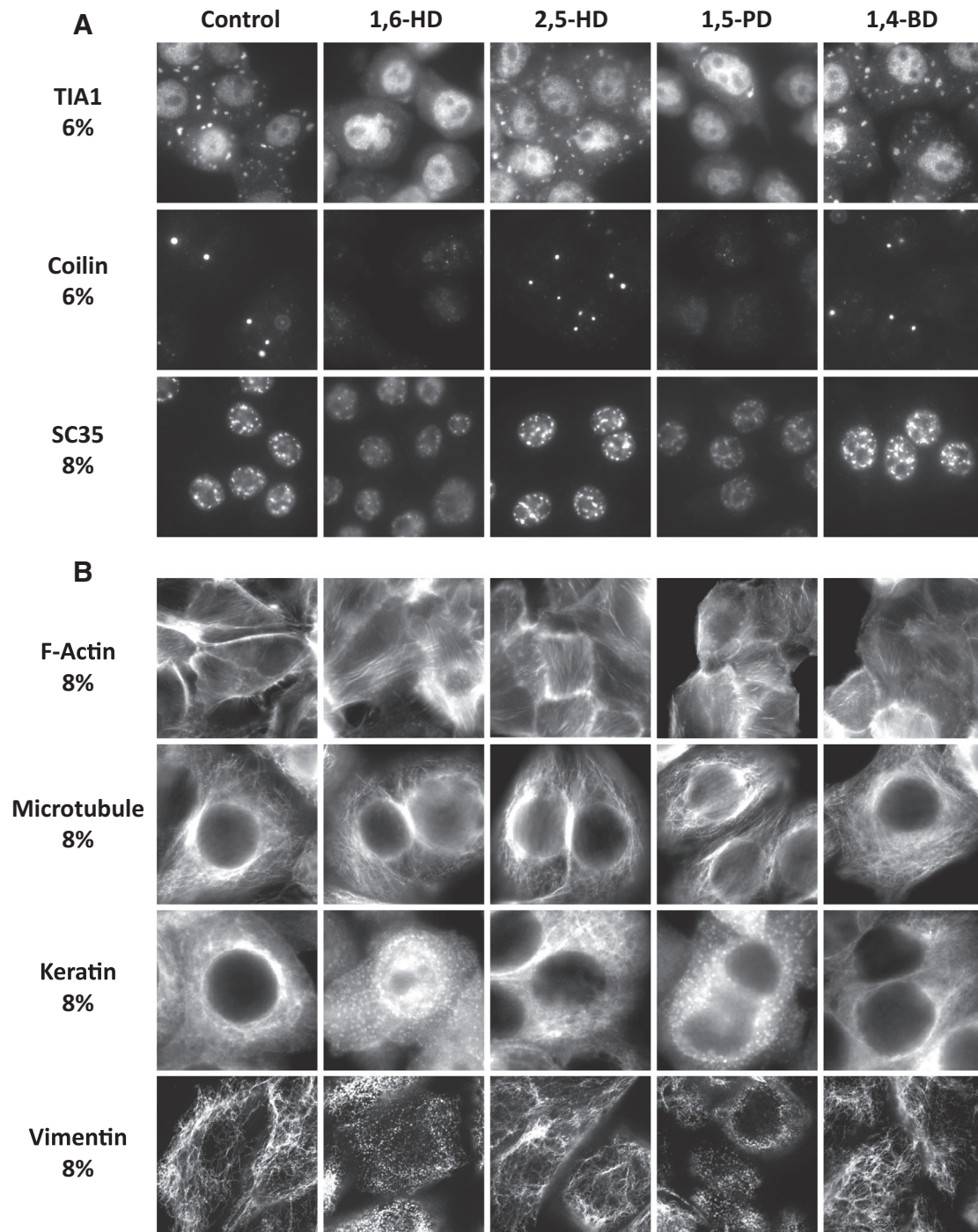


**Figure 3. Effects of Aliphatic Alcohols on RNA Granules, Cajal Bodies, Nuclear Speckles, and Cytoskeletal Filaments**

(A) HeLa cells were exposed to indicated aliphatic alcohols for 5 min, fixed and stained with antibodies diagnostic of stress granules (TIA1), Cajal bodies (coilin) or nuclear speckles (SC35).

(B) HeLa cells were exposed to indicated aliphatic alcohols for 5 min, fixed and stained with either dye-labeled phalloidin or antibodies to tubulin, keratin or vimentin.

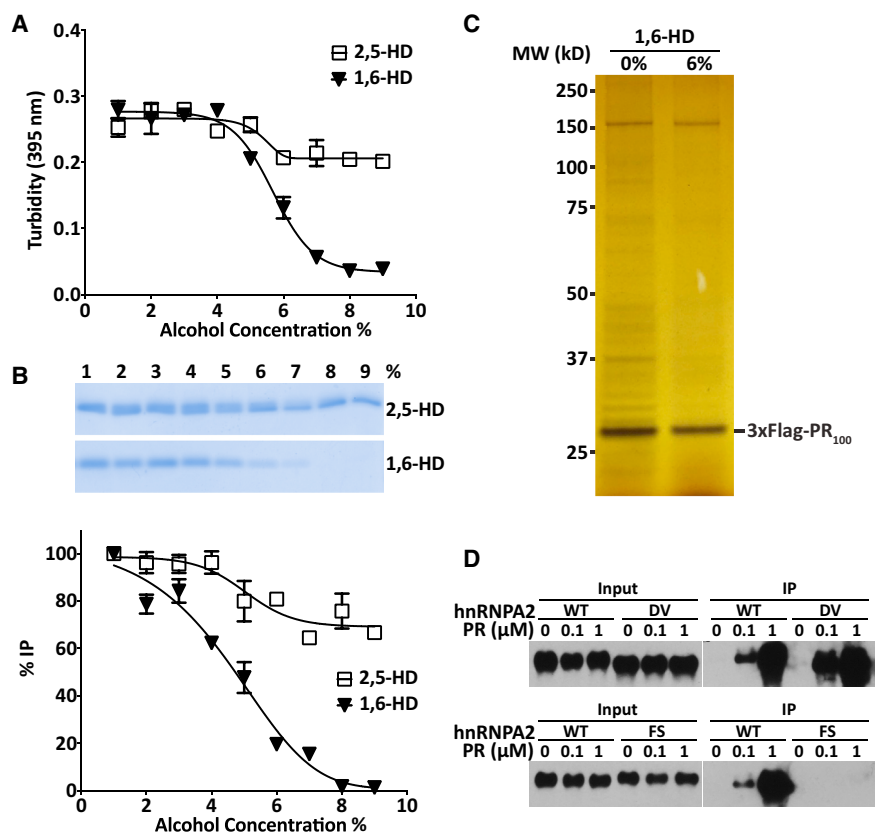


**Figure 4. Effects of Aliphatic Alcohols on Interactions between the PR<sub>n</sub> Poly-Dipeptide and Its Cellular Targets**

(A) Turbidity of hnRNPA2 low complexity polymers in response to indicated concentrations of either 1,6-hexanediol or 2,5-hexanediol as measured by light scattering at 395 nm ( $n = 2$ , data are presented as means  $\pm$  SD).

(B) Coomassie stained SDS-PAGE gel of immunoprecipitated samples of the low complexity domain of hnRNPA2 by the PR<sub>20</sub>:HA probe as a function of exposure to between 1% and 9% of the indicated aliphatic alcohol. Band intensities were quantified from SDS-PAGE gel (top) by ImageJ, and then plotted (bottom) ( $n = 2$ , data are presented as means  $\pm$  SD).

(C) Silver stained SDS-PAGE gel of immunoprecipitated proteins from U2OS cells expressing the 3xFlag:PR<sub>100</sub> protein. Left lane shows proteins co-precipitated in the absence of aliphatic alcohols, right lane shows proteins co-precipitated in the presence of 6% 1,6-hexanediol (see also Figure S3).

(D) Western blots showing native hnRNPA2 protein or variants bearing single amino acid substitutions (DV = aspartic acid residue 290 changed to valine, or FS = phenylalanine residue 291 changed to serine) as input to immunoprecipitation reactions (left panels), or as immunoprecipitated in response to varying concentrations of the PR<sub>20</sub>:HA probe (right panels) (see also Figure S4).

### PR<sub>n</sub> Poly-Dipeptides Bind the Head Domains of Intermediate Filament Proteins

Mammalian genomes encode upward of 70 different types of intermediate filaments. These proteins contain centrally located alpha helical domains that initially align in parallel to form coiled-coil dimers. Dimers further associate in an anti-parallel manner to form tetramers, and fully assembled intermediate filaments organize eight tetramers to form their long, cylindrical morphology (Herrmann et al., 2007). All intermediate filaments contain LC domains on both the amino- and carboxyl-terminal sides of the central coiled coil domain. The amino-terminal LC sequences of intermediate filament proteins are referred to as head domains, the carboxyl-terminal LC sequences are termed tail domains. Conversion of coiled-coil tetramers into fully assembled intermediate filaments is critically dependent upon the head domain, yet can proceed in certain instances in the absence of the tail domain (Hatzfeld and Burba, 1994; Herrmann et al., 1996).

The head domains of intermediate filaments range in size from 60–150 amino acids and have been characterized as intrinsically disordered sequences that function in a structure-independent manner (Castaing and Harf, 1986). The tail domains of intermediate filaments vary widely in size, and have also been characterized as intrinsically disordered and of low complexity with regard to amino acid sequence.

Isolated head and tail domains of various intermediate filaments, including vimentin, peripherin, and the light, medium

and heavy isoforms of neurofilaments, were fused to mCherry, expressed, purified, and incubated under conditions suitable for LC domain polymerization. All five fusion proteins linking the head domains of intermediate filaments to mCherry were observed to polymerize and gel (Figures 5A and S5A). Fibrous polymers of the head domains of vimentin, peripherin, and all three neurofilament isoforms revealed X-ray diffraction rings of 4.7 and 10 Å prototypic of cross- $\beta$  amyloid fibers, and were labile to depolymerization upon dilution as deduced by SDD-AGE (Figures S5B and S5C). Using the same experimental conditions, no evidence of polymerization was observed for mCherry fusion proteins linked to the tail domains of vimentin, peripherin, or any of the three neurofilament isoforms.

Hydrogel droplets composed of labile amyloid-like fibers formed from the head domains of either vimentin or the light chain neurofilament protein were probed with both GFP and the GFP derivative linked to twenty repeats of the PR<sub>n</sub> poly-dipeptide (GFP:PR<sub>20</sub>). The former protein penetrated the porous hydrogel droplets but was not bound. By contrast, GFP:PR<sub>20</sub> bound avidly to both mCherry:vimentin and mCherry:neurofilament hydrogel droplets (Figure 5A).

### Hierarchical Melting of Intermediate Filaments by Aliphatic Alcohols

Polymers composed of the head domain of vimentin fused to mCherry melted in response to 1,6-HD, but not the related 2,5-HD (Figure 5B). Similarly selective fibril melting by 1,6-HD was

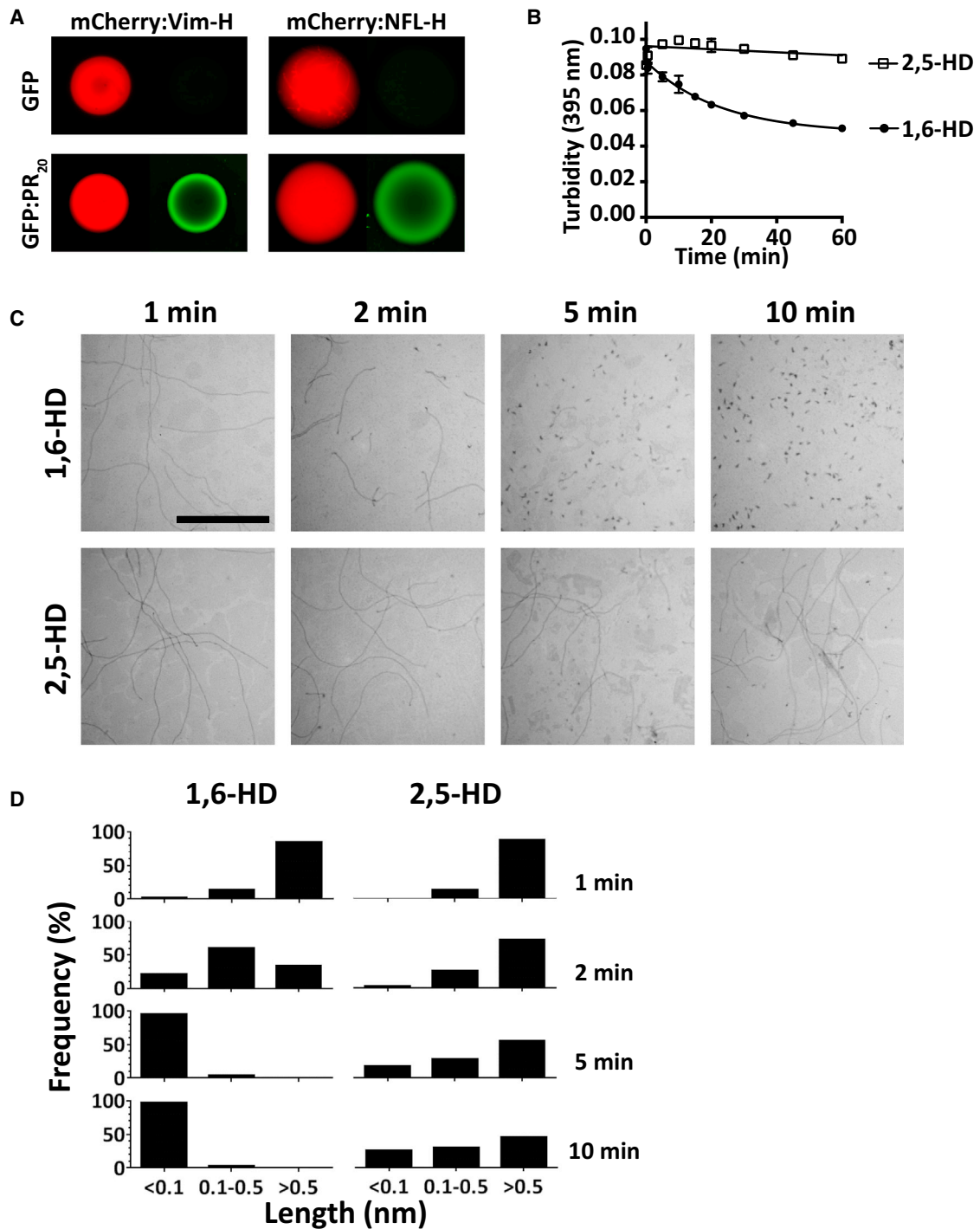


**Figure 5. Binding of GFP:PR<sub>20</sub> to mCherry:IF Head Domain Hydrogel, and Sensitivity of Vimentin Intermediate Filaments to Aliphatic Alcohols**  
 (A) Hydrogel droplets containing fusion proteins made from mCherry linked to the low complexity head domains of vimentin (left) or neurofilament light isoform (right) were incubated with either GFP (top images) or GFP:PR<sub>20</sub> (lower images) and visualized by confocal microscopy (STAR Methods) (see also Figure S5).  
 (B) Turbidity measurements as determined by light scattering at 395 nm of polymers formed from an mCherry:vimentin head domain fusion protein in response to 15% of indicated aliphatic alcohols for indicated times (n = 3) data are presented as means ± SD. Note that error bars for most of the data points are smaller than the symbols (see also Figure S6A).  
 (C) Electron microscope images of vimentin intermediate filament proteins exposed to indicated aliphatic alcohols for indicated times, scale bar = 1 μm (see also Figure S6B).  
 (D) Quantitation of lengths of intermediate filaments as a function of exposure to indicated aliphatic alcohols for indicated times.

also observed for polymers formed from mCherry fusion proteins linked to the head domains of peripherin, and all three isoforms of neurofilaments (Figure S6A).

The effects of aliphatic alcohols were further tested on purified microtubules, actin filaments, and intermediate filaments as visualized by transmission electron microscopy. Neither 1,6-HD nor 2,5-HD affected the length or integrity of either microtubules or actin filaments even after an exposure time of 30 min (Figure S6B). By contrast, 1,6-HD caused rapid disassembly of vimentin intermediate filaments (Figures 5C and 5D). Within 2 min post-exposure, filament length was significantly reduced, and filaments were fully disassembled into punctate dots within 5 min. Exposure of vimentin intermediate filaments to the same concentration (2.5%) of the related aliphatic alcohol, 2,5-HD, did not significantly affect filament length or morphology (Figures 5C and 5D). These findings give evidence that the two aliphatic alcohols display the same pattern of effects on isolated cytoskeletal proteins as compared with the same filaments in living cells (Figure 3).

#### GFP:PR<sub>20</sub> and GFP:FUS Bind as Repetitive Puncta along Vimentin Intermediate Filaments

Vimentin intermediate filaments were prepared from the intact protein, exposed to one of three test proteins, and rapidly deposited onto electron microscope grids (STAR Methods). When exposed to GFP, no change in intermediate filament morphology was observed. By contrast, when vimentin intermediate filaments were exposed to the GFP variant fused to 20 repeats of the PR<sub>n</sub> poly-dipeptide (GFP:PR<sub>20</sub>), repetitive knobs were observed to decorate the filaments (Figure 6A). Similar treatment of either microtubules or actin filaments with the GFP:PR<sub>20</sub> fusion protein failed to alter fiber morphology (Figure S6C). Repetitive particles also decorated vimentin intermediate filaments exposed to a fusion protein linking the LC domain of FUS to GFP (Figure 6A).

The knob-to-knob distance of 1,000 particles observed to decorate vimentin intermediate filaments exposed to GFP:PR<sub>20</sub> measured  $47.0 \pm 13.5$  nm (Figures 6B and 6C). Small angle X-ray scattering studies of intermediate filaments have led to the conclusion that the head and tail LC domains are distributed along intermediate filaments with a periodicity of 46 nm (Mücke et al., 2004; Sokolova et al., 2006). We tentatively conclude that the GFP:PR<sub>20</sub> and GFP:FUS fusion proteins bind to intermediate filaments via direct interaction with the periodic repeats where head and tail LC domains converge along the length of intermediate filaments.

Inspection of micrographs, of which Figure 6B is representative, gave evidence of two categories of vimentin-interacting puncta. Both, we propose, correspond to aggregates of the GFP:PR<sub>20</sub> fusion protein. The majority of vimentin-bound puncta were 15–20 nm in diameter. At roughly 10% of the frequency of this predominant category of puncta, we observed GFP:PR<sub>20</sub> aggregates of roughly double the normal size (Figure 6D). Images were evaluated for the frequency of vimentin-bound puncta proximal to either of these two size categories. As shown in Figure 6E, approximately 80% of the smaller puncta displayed a neighboring protein aggregate within 60 nm along the vimentin filament. By contrast, only 20%–30% of the larger puncta were

found to be proximal to another PR<sub>n</sub> protein aggregate. Although we do not understand why this might be, we offer the interpretation that the larger protein aggregates have assimilated one or more neighboring particles in proximity along the axis of the vimentin filament. This simplistic idea might account for both variation in aggregate size and the paucity of puncta neighboring the larger aggregates.

Derivatives of vimentin missing LC sequences specifying the N-terminal head domain, or the C-terminal tail domain, were expressed in bacteria, purified and assayed for assembly into intermediate filaments (STAR Methods). Consistent with the observations of others (Herrmann et al., 1996), the headless variant of vimentin failed to form intermediate filaments, yet the tail-less variant did assemble into intermediate filaments. When incubated with GFP:PR<sub>20</sub>, these tail-less filaments failed to become decorated with periodic puncta upon exposure to the GFP:PR<sub>20</sub> fusion protein (Figure S6D). Such data give evidence that LC sequences associated with both head and tail domains may be required for GFP:PR<sub>20</sub> to coalesce into puncta along the axial length of vimentin intermediate filaments.

#### DISCUSSION

The work described in this article covers three related phenomena. First, we have used several methods in search of the intracellular targets of the toxic PR<sub>n</sub> poly-dipeptide encoded by the C9orf72 repeat expansion. Both photo-crosslinking and affinity purification methods revealed PR<sub>n</sub> interaction with a variety of cellular proteins (Tables S1 and S2). Whereas nuclear and cytoplasmic puncta not surrounding by investing membranes and intermediate filaments topped the list of PR<sub>n</sub>-bound proteins, we also observed interaction with proteins involved in many other aspect of cell organization and function. We therefore conclude that the PR<sub>n</sub> poly-dipeptide exerts its toxicity by interfering with multiple features of cellular physiology and function.

Domains of low complexity (LC) sequence are shared by many targets of the toxic PR<sub>n</sub> poly-dipeptide. For the hnRNPA1 protein, it was possible to demonstrate that its LC domain was both necessary and sufficient for PR<sub>n</sub> binding (Figure 1D). We have provided several lines of evidence indicative of polymer-dependent binding of the PR<sub>n</sub> poly-dipeptide to certain of its targets. Either pharmacologic or mutational disruption of LC domain polymers impeded PR<sub>n</sub> interaction with the hnRNPA2 RNA binding protein (Figures 4B and 4D). Likewise, the conditionally-induced 3xFlag:PR<sub>100</sub> protein failed to co-precipitate its intracellular targets when cellular lysates were exposed to a polymer melting aliphatic alcohol (1,6-HD) (Figure 4C). We interpret polymer dependence to reflect the idea that iterative PR repeats can exploit their inherent multi-valency when bound to polymeric targets that themselves offer iteratively repeated epitopes for PR interaction. This simplistic interpretation is at odds with numerous other studies that consider labile LC domain polymers to be of no biologic utility (Bergeron-Sandoval et al., 2016; Guo and Shorter, 2015; Wu and Fuxreiter, 2016).

A second feature of this work concerns the effects of aliphatic alcohols on the integrity of cellular structures not invested by surrounding membranes as compared with the abilities of the same alcohols to disassemble cross- $\beta$  polymers formed from

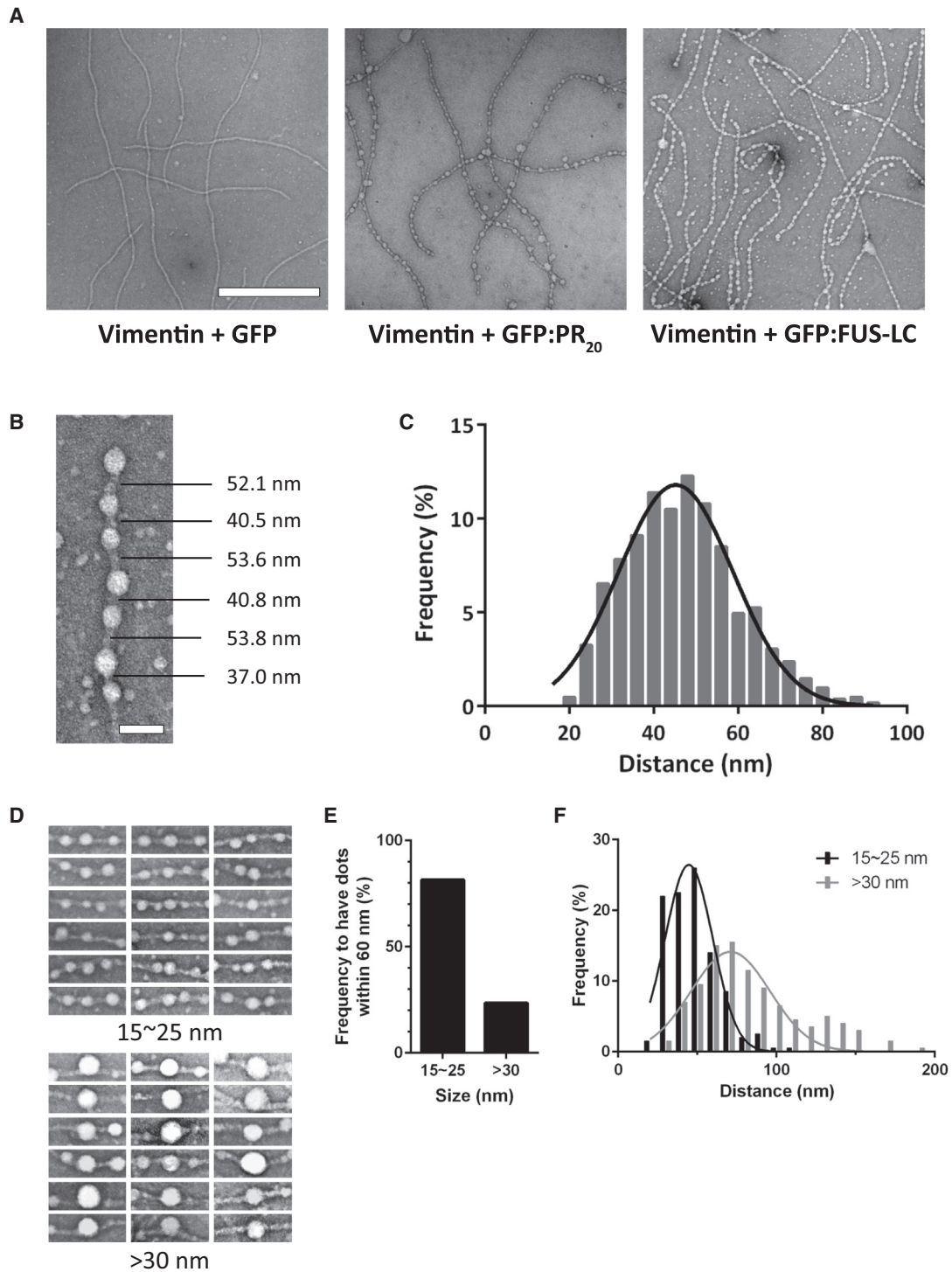


**Figure 6. GFP:PR<sub>20</sub> and GFP:FUS Bind Periodically to Vimentin Intermediate Filaments**

(A) Electron microscope images of vimentin intermediate filaments exposed to GFP (left), GFP:PR<sub>20</sub> (middle) or GFP:FUS (right). Scale bar = 500 nm (see also Figures S6C and S6D).

(B) Representative image showing the puncta-to-puncta distance of GFP:PR<sub>20</sub> bound to a single vimentin intermediate filament. Scale bar = 50 nm.

(C) Quantification of puncta-to-puncta distances of GFP:PR<sub>20</sub> bound to vimentin intermediate filaments (n = 1,000). The curve was fitted by Gaussian distribution.

(D) Representative images of different sized puncta (15~25 nm or > 30 nm) of GFP:PR<sub>20</sub> bound to vimentin intermediate filaments.

(E) Quantification of frequency to have puncta of GFP:PR<sub>20</sub> puncta within 60 nm of small or large puncta.

(F) Quantification of puncta-to-puncta distance of GFP:PR<sub>20</sub> bound to vimentin intermediate filaments as a function of puncta size. p < 0.001 (n = 200)

LC sequences. Cellular structures including RNA granules, Cajal bodies, nuclear speckles, and intermediate filaments were dissolved effectively by 1,6-HD, less so by 1,5-PD, but not by 2,5-HD or 1,4-BD (Figure 3). A similar pattern of effects was observed with respect to the abilities of these aliphatic alcohols to melt both hydrogels composed of LC polymers and liquid-like droplets formed in part via the chemical properties of the LC domains of FUS and hnRNPA2 (Figure 2). That aliphatic alcohols melt cellular puncta and intermediate filaments in a manner correlative to the melting of LC domain polymers is supportive of the thesis that cross- $\beta$  polymerization of LC sequences may be broadly employed to facilitate cell organization (Han et al., 2012; Kato et al., 2012).

The means by which aliphatic alcohols melt membrane-free cellular bodies and polymeric fibers formed from LC domains remains enigmatic. Among the four aliphatic alcohols used in these studies, 1,6-HD is the most hydrophobic as assessed by four different computational measures (Table S4). Hydrophobicity alone, however, may not account for the hierarchical abilities of the four aliphatic alcohols to melt membrane-free organelles, intermediate filaments, and cross- $\beta$  polymers. All four measures of hydrophobicity predict 2,5-HD to be more hydrophobic than 1,5-PD, yet the former chemical is considerably less active than the latter in all assays performed herein.

In an extended conformation, the hydroxyl groups on either end of 1,6-HD are separated by 10 Å. X-ray diffraction analyses of cross- $\beta$  polymers formed from the LC domains of hnRNPA2 and FUS reveal diffraction rings at 4.6/4.7 and 10 Å (Kato et al., 2012). The former ring corresponds to the distance separating aligned subunits along the fibril axis and is invariant in cross- $\beta$  polymers (Astbury et al., 1935; Marsh et al., 1955). The latter, 10 Å diffraction ring likely corresponds to some element of structure built within individual polypeptide subunits. In the many cross- $\beta$ , amyloid-like fibers characterized over the past half-century, the dimensions of these intra-peptide interactions vary from 6 to 11 Å (Greenwald and Riek, 2010). For reasons we do not yet understand, all of the LC domain polymers we have studied to date—including the five new examples shown in Figure S5—reveal an invariant 10 Å diffraction ring. We speculate that the matching, 10 Å dimensions of the extended conformation of 1,6-HD, coupled with its inherent hydrophobicity, may hint as to why this particular aliphatic alcohol is most effective in melting cross- $\beta$  polymers formed from the LC domains we have studied to date.

The third and most surprising aspect of this work concerns the finding that the PR<sub>n</sub> poly-dipeptide may interact directly with intermediate filaments. Studies of recombinant vimentin revealed that this interaction involves PR<sub>n</sub> binding to the amino-terminal head domain (Figure 5A). The vimentin head domain is of low complexity and forms labile, cross- $\beta$  polymers selectively sensitive to dissolution by 1,6-HD. These observations raise the possibility that the dynamic behavior of intermediate filaments may be informed by our earlier conceptualizations regarding cellular puncta not invested by surrounding membranes (Han et al., 2012; Kato et al., 2012).

The head and tail LC domains of intermediate filaments are well-known targets of phosphorylation (Eriksson et al., 2004; Geisler et al., 1989), and mutations in the head domains of neuro-

filament proteins have been causally linked to certain forms of neurodegenerative disease (Brownlee et al., 2002; Fabrizi et al., 2004; Georgiou et al., 2002; Perez-Olle et al., 2004; Shin et al., 2008). We speculate that the dynamic behavior of intermediate filaments may be influenced both by post-translational modifications that impede cross- $\beta$  interactions involving head domains, or mutations that improperly stabilize polymers.

It may be useful to compare these studies with recent observations coming from the laboratories of Anne Ephrussi (Gaspar et al., 2016) and Denise Montell (Cho et al., 2016). Mutations affecting deposition of polar granules in fruit fly eggs have recently been understood to act by blocking the formation of an alternatively spliced variant of tropomyosin. Unlike the conventional tropomyosin well understood to participate in the actin cytoskeleton, the spliced variant critical for polar granule deposition contains LC domains on the amino- and carboxyl-terminal sides of the tropomyosin coiled coil domain. Other than nuclear lamins, the *Drosophila melanogaster* genome does not encode intermediate filament proteins. The beautiful work from the Ephrussi and Montell labs reveals an alternatively spliced tropomyosin variant that is, for all intents and purposes, an intermediate filament protein critical for proper deposition of polar granules and germ cell specification.

Interactions between the LC domains of RNA granule proteins and intermediate filaments may be centrally involved in the control of localized translation. Studies concerning the selective deposition of the Veg1 mRNA within the vegetal hemisphere of *Xenopus laevis* oocytes upward of three decades ago revealed interaction with intermediate filament proteins (Pondel and King, 1988). Polar asymmetry of the frog egg has been beautifully correlated with asymmetry in the organization of cortical intermediate filaments (Klymkowsky et al., 1987). Intriguingly, punctate staining of the vegetal pole of *Xenopus* eggs has been observed with two distinct antibodies that selectively bind to amyloid polymers (Hayes and Weeks, 2016). Finally, it has been reported that asymmetric partitioning of vimentin intermediate filaments during cell division may facilitate asymmetric partitioning of puncta composed of aggregated proteins (Ogrodnik et al., 2014).

Proper spatial partitioning of RNA granules is particularly important to nerve cells. We speculate that neuronal granules used to facilitate localized translation in the vicinity of active synapses might employ interactions with the LC domains arranged periodically along the length of neurofilaments. The electron microscope images of GFP:PR<sub>20</sub> and GFP:FUS binding to vimentin are interpreted to give evidence that puncta, possibly representative of RNA granules, might pass longitudinally from transient interaction with one zone of low complexity sequence to another along intermediate filaments (Figure 6). Whereas these interactions would not offer any means of establishing directionality to the movement of neuronal granules along neuronal appendages, they might offer a confining advantage to the process. Given the close apposition of neurofilaments to microtubules that themselves align parallel to nerve cell appendages (Chang and Goldman, 2004; Fletcher and Mullins, 2010; Schnapp and Reese, 1982), the proximal combination of these two forms of cytoskeletal filaments might conspire to facilitate movement of neuronal granules to the appropriate subcellular

compartments. Proper trafficking of neuronal granules to the synapses of neurons might be impeded were the PR<sub>n</sub> poly-dipeptide to bind to LC domains associated with neurofilament proteins.

Finally, we offer that our concept of PR<sub>n</sub>-mediated toxicity aligns with interpretations coming from a wide spectrum of studies of human mutations causative of neurodegenerative disease. Mutations in the LC domains of RNA binding proteins are beginning to be understood to abet the stability of cross- $\beta$  polymers (Kim et al., 2013; Patel et al., 2015; Vieira et al., 2014). Our own studies of D-to-V mutations in three different hnRNPs give evidence that the inherent tuning of LC domains between monomeric and polymeric state can be significantly impacted by single amino acid changes causative of human disease (Figure S4). We speculate that binding of the toxic PR<sub>n</sub> poly-dipeptide to otherwise labile cross- $\beta$  polymers associated with membrane-free cellular organelles and intermediate filaments might also cause an imbalance in polymer stability. If correct, this conceptualization may offer a unified means of considering mechanisms of pathogenicity for a broad spectrum of neurodegenerative diseases.

## STAR★METHODS

Detailed methods are provided in the online version of this paper and include the following:

- KEY RESOURCES TABLE
- CONTACT FOR REAGENT AND RESOURCE SHARING
- METHOD DETAILS
  - Synthesis of PR<sub>20</sub>HA and PR<sub>20</sub>BAH Peptide
  - Live-Cell Crosslinking Using PR<sub>20</sub>BAH Probe
  - Construction of Flag-PR<sub>100</sub>-HA Stable Cell Line
  - Cryogenic Extraction and Affinity Purification of PR<sub>100</sub>
  - Proteomic Analysis and Computation Analysis of LC Sequences
  - Immunoprecipitation of hnRNPA1 Domain Constructs
  - Preparation of GFP- and mCherry-Fusion Proteins
  - Preparation and Characterization of Fibers/Hydrogels
  - Melting of Fibers/Hydrogels by Aliphatic Alcohols
  - Melting of Sub-cellular Structures by Aliphatic Alcohols
  - Melting of PTB:hnRNPA2 LC Liquid-Like Droplets by Aliphatic Alcohols
  - Immunoprecipitation of hnRNPA2 LCS in the Presence of Aliphatic Alcohols
  - Assembly of Recombinant Vimentin Intermediate Filaments
  - Assembly of Actin and Tubulin Filaments
  - Melting of Filaments by Aliphatic Alcohols
  - GFP:PR<sub>20</sub> Binding to Cytoskeletal Filaments
  - Hydrophobicity Analysis of Aliphatic Alcohols
- QUANTIFICATION AND STATISTICAL ANALYSIS

## SUPPLEMENTAL INFORMATION

Supplemental Information includes six figures, four tables, and one movie and can be found with this article online at <http://dx.doi.org/10.1016/j.cell.2016.10.003>.

## AUTHOR CONTRIBUTIONS

I.K. and Y.L. contributed to Figure 1A. Y. L. contributed to Figures 1B–1D, Figure 4 and Figure S3. E.M. contributed to Figures 5C and 5D, Figure 6, and Figures S6C and S6D. M.K. contributed to Figures 2A–2C, Figures 5A–5B, and Figures S2, S4, S5, and S6A. S.X. contributed to Figures 2D and 2E, Figure 3, and Figure S6B. S.X. contributed to Figures 2D and 2E and Figure 3. L.W. made all DNA constructs. S.M. planned the experiments, analyzed the data and prepared the manuscript with input from all authors.

## ACKNOWLEDGMENTS

We thank Drs. Richard Losick, Ruth Lehmann, Deepak Nijhawan and Ting Han for valuable input; Dr. Robert Tycko of the National Institutes of Health for provision of A $\beta$ -40 in the polymeric, prion state; Dr. Randal Halfmann of Stowers Institute for provision of sup35 in the polymeric, prion state; Drs. Joseph Ready and Hayden Ball for help in synthesis of the benzophenone-labeled PR<sub>20</sub> peptide; Drs. Anne Ephrussi and Denise Montell for communication of unpublished observations concerning their co-discovery of a spliced variant of *Drosophila melanogaster* tropomyosin having intermediate filament-like properties; Dr. Luke Rice for provision of pocine brain tubulin; the Live Cell Imaging and Electron Microscopy Core Laboratories at UTSWMC for technical assistance; and the Nijhawan laboratory at UTSWMC for technical advice and access to equipment for preparing cryo-mill-generated cellular lysates. This work was supported by the National Research Foundation of Korea (NRF) grants (#2016R1C1B2008776 and #2016R1A4A1011189) awarded IK by the Korean government, grant #5UO1-GM107623-02 awarded SLM from the National Institute of General Medical Sciences, and unrestricted funds provided to SLM by an anonymous donor.

Received: May 31, 2016

Revised: August 8, 2016

Accepted: September 30, 2016

Published: October 20, 2016

## REFERENCES

- ACD/Structure Elucidator (2015). version 15.01, Advanced Chemistry Development, Inc., Toronto, ON, Canada, <http://www.acdlabs.com/>.
- Ash, P.E., Bieniek, K.F., Gendron, T.F., Caulfield, T., Lin, W.L., DeJesus-Hernandez, M., van Blitterswijk, M.M., Jansen-West, K., Paul, J.W., 3rd, Rademakers, R., et al. (2013). Unconventional translation of C9ORF72 GGGGCC expansion generates insoluble polypeptides specific to c9FTD/ALS. *Neuron* 77, 639–646.
- Astbury, W.T., Dickinson, S., and Bailey, K. (1935). The X-ray interpretation of denaturation and the structure of the seed globulins. *Biochem J* 29, 2351–2360, 2351.
- Bergeron-Sandoval, L.P., Safaee, N., and Michnick, S.W. (2016). Mechanisms and Consequences of Macromolecular Phase Separation. *Cell* 165, 1067–1079.
- Brownlee, J., Ackerley, S., Grierson, A.J., Jacobsen, N.J., Shea, K., Anderton, B.H., Leigh, P.N., Shaw, C.E., and Miller, C.C. (2002). Charcot-Marie-Tooth disease neurofilament mutations disrupt neurofilament assembly and axonal transport. *Hum. Mol. Genet.* 11, 2837–2844.
- Castaing, Y., and Harf, A. (1986). [Evaluation of the distribution of pulmonary ventilation-perfusion ratios]. *Rev. Mal. Respir.* 3, 399–403.
- Chang, L., and Goldman, R.D. (2004). Intermediate filaments mediate cytoskeletal crosstalk. *Nat. Rev. Mol. Cell Biol.* 5, 601–613.
- Cho, A., Kato, M., Whitwam, T., Kim, J.H., and Montell, D.J. (2016). An Atypical Tropomyosin in *Drosophila* with Intermediate Filament-like Properties. *Cell Rep.* 16, 928–938.
- DeJesus-Hernandez, M., Mackenzie, I.R., Boeve, B.F., Boxer, A.L., Baker, M., Rutherford, N.J., Nicholson, A.M., Finch, N.A., Flynn, H., Adamson, J., et al. (2011). Expanded GGGGCC hexanucleotide repeat in noncoding region of C9ORF72 causes chromosome 9p-linked FTD and ALS. *Neuron* 72, 245–256.

- Donnelly, C.J., Zhang, P.W., Pham, J.T., Haeusler, A.R., Mistry, N.A., Viden-sky, S., Daley, E.L., Poth, E.M., Hoover, B., Fines, D.M., et al. (2013). RNA toxicity from the ALS/FTD C9ORF72 expansion is mitigated by antisense inter-vention. *Neuron* 80, 415–428.
- Dyson, H.J., and Wright, P.E. (2005). Intrinsically unstructured proteins and their functions. *Nat. Rev. Mol. Cell Biol.* 6, 197–208.
- Eriksson, J.E., He, T., Trejo-Skalli, A.V., Härmälä-Braskén, A.S., Hellman, J., Chou, Y.H., and Goldman, R.D. (2004). Specific in vivo phosphorylation sites determine the assembly dynamics of vimentin intermediate filaments. *J. Cell Sci.* 117, 919–932.
- Fabrizi, G.M., Cavallaro, T., Angiari, C., Bertolasi, L., Cabrini, I., Ferrarini, M., and Rizzuto, N. (2004). Giant axon and neurofilament accumulation in Char-cot-Marie-Tooth disease type 2E. *Neurology* 62, 1429–1431.
- Fletcher, D.A., and Mullins, R.D. (2010). Cell mechanics and the cytoskeleton. *Nature* 463, 485–492.
- Freibaum, B.D., Lu, Y., Lopez-Gonzalez, R., Kim, N.C., Almeida, S., Lee, K.H., Badders, N., Valentine, M., Miller, B.L., Wong, P.C., et al. (2015). GGGGCC repeat expansion in C9orf72 compromises nucleocytoplasmic transport. *Nature* 525, 129–133.
- Gaspar, I., Sysoev, V., Komissarov, A., and Ephrussi, A. (2016). An RNA-bind-ing tropomyosin recruits kinesin-1 dynamically to oskar mRNPs. *bioRxiv*. <http://dx.doi.org/10.1101/067876>.
- Geisler, N., Hatzfeld, M., and Weber, K. (1989). Phosphorylation in vitro of vimentin by protein kinases A and C is restricted to the head domain. Identifi-cation of the phosphoserine sites and their influence on filament formation. *Eur. J. Biochem.* 183, 441–447.
- Georgiou, D.M., Zidar, J., Korosec, M., Middleton, L.T., Kyriakides, T., and Christodoulou, K. (2002). A novel NF-L mutation Pro22Ser is associated with CMT2 in a large Slovenian family. *Neurogenetics* 4, 93–96.
- Greenwald, J., and Riek, R. (2010). Biology of amyloid: structure, function, and regulation. *Structure* 18, 1244–1260.
- Guo, L., and Shorter, J. (2015). It's Raining Liquids: RNA Tunes Viscoelasticity and Dynamics of Membraneless Organelles. *Mol. Cell* 60, 189–192.
- Haeusler, A.R., Donnelly, C.J., Periz, G., Simko, E.A., Shaw, P.G., Kim, M.S., Maragakis, N.J., Troncoso, J.C., Pandey, A., Sattler, R., et al. (2014). C9orf72 nucleotide repeat structures initiate molecular cascades of disease. *Nature* 507, 195–200.
- Han, T.W., Kato, M., Xie, S., Wu, L.C., Mirzaei, H., Pei, J., Chen, M., Xie, Y., Allen, J., Xiao, G., and McKnight, S.L. (2012). Cell-free formation of RNA gran-ules: bound RNAs identify features and components of cellular assemblies. *Cell* 149, 768–779.
- Hatzfeld, M., and Burba, M. (1994). Function of type I and type II keratin head domains: their role in dimer, tetramer and filament formation. *J. Cell Sci.* 107, 1959–1972.
- Hayes, M.H., and Weeks, D.L. (2016). Amyloids assemble as part of recogniz-able structures during oogenesis in *Xenopus*. *Biol. Open* 5, 801–806.
- Herrmann, H., Häner, M., Brettel, M., Müller, S.A., Goldie, K.N., Fedtke, B., Lustig, A., Franke, W.W., and Aebi, U. (1996). Structure and assembly prop-erties of the intermediate filament protein vimentin: the role of its head, rod and tail domains. *J. Mol. Biol.* 264, 933–953.
- Herrmann, H., Bär, H., Kreplak, L., Strelkov, S.V., and Aebi, U. (2007). Interme-diate filaments: from cell architecture to nanomechanics. *Nat. Rev. Mol. Cell Biol.* 8, 562–573.
- Jovičić, A., Mertens, J., Boeynaems, S., Bogaert, E., Chai, N., Yamada, S.B., Paul, J.W., 3rd, Sun, S., Herdy, J.R., Bieri, G., et al. (2015). Modifiers of C9orf72 dipeptide repeat toxicity connect nucleocytoplasmic transport defects to FTD/ALS. *Nat. Neurosci.* 18, 1226–1229.
- Kato, M., Han, T.W., Xie, S., Shi, K., Du, X., Wu, L.C., Mirzaei, H., Goldsmith, E.J., Longgood, J., Pei, J., et al. (2012). Cell-free formation of RNA granules: low complexity sequence domains form dynamic fibers within hydrogels. *Cell* 149, 753–767.
- Kim, H.J., Kim, N.C., Wang, Y.D., Scarborough, E.A., Moore, J., Diaz, Z., MacLea, K.S., Freibaum, B., Li, S., Molliex, A., et al. (2013). Mutations in prion-like domains in hnRNPA2B1 and hnRNPA1 cause multisystem protein-opathy and ALS. *Nature* 495, 467–473.
- Klymkowsky, M.W., Maynell, L.A., and Polson, A.G. (1987). Polar asymmetry in the organization of the cortical cyokeratin system of *Xenopus laevis* oocytes and embryos. *Development* 100, 543–557.
- Kroschwald, S., Maharana, S., Mateju, D., Malinowska, L., Nüske, E., Poser, I., Richter, D., and Alberti, S. (2015). Promiscuous interactions and protein disag-gregases determine the material state of stress-inducible RNP granules. *eLife* 4, e06807.
- Kwon, I., Xiang, S., Kato, M., Wu, L., Theodoropoulos, P., Wang, T., Kim, J., Yun, J., Xie, Y., and McKnight, S.L. (2014). Poly-dipeptides encoded by the C9orf72 repeats bind nucleoli, impede RNA biogenesis, and kill cells. *Science* 345, 1139–1145.
- Lagier-Tourenne, C., Baughn, M., Rigo, F., Sun, S., Liu, P., Li, H.R., Jiang, J., Watt, A.T., Chun, S., Katz, M., et al. (2013). Targeted degradation of sense and antisense C9orf72 RNA foci as therapy for ALS and frontotemporal degenera-tion. *Proc. Natl. Acad. Sci. USA* 110, E4530–E4539.
- Lee, Y.B., Chen, H.J., Peres, J.N., Gomez-Deza, J., Attig, J., Stalekar, M., Troakes, C., Nishimura, A.L., Scotter, E.L., Vance, C., et al. (2013). Hexanu-cleotide repeats in ALS/FTD form length-dependent RNA foci, sequester RNA binding proteins, and are neurotoxic. *Cell Rep.* 5, 1178–1186.
- Lee, K.-H., Zhang, P., Mitrea, D., Sarkar, M., Freibaum, B., Cika, J., Coughlin, M., Messing, J., Molliex, A., Maxwell, B., et al. (2016). C9orf72 Dipeptide Repeats Impair the Assembly, Dynamics, and Function of Membrane-Less Organelles. *Cell* 167, this issue, 774–788.
- Lin, Y., Protter, D.S., Rosen, M.K., and Parker, R. (2015). Formation and Matu-ration of Phase-Separated Liquid Droplets by RNA-Binding Proteins. *Mol. Cell* 60, 208–219.
- Marsh, R.E., Corey, R.B., and Pauling, L. (1955). An investigation of the struc-ture of silk fibroin. *Biochim. Biophys. Acta* 16, 1–34.
- Mizielinska, S., Lashley, T., Norona, F.E., Clayton, E.L., Ridler, C.E., Fratta, P., and Isaacs, A.M. (2013). C9orf72 frontotemporal lobar degeneration is charac-terised by frequent neuronal sense and antisense RNA foci. *Acta Neuropathol.* 126, 845–857.
- Mizielinska, S., Grönke, S., Niccoli, T., Ridler, C.E., Clayton, E.L., Devoy, A., Moens, T., Norona, F.E., Woollacott, I.O., Pietrzyk, J., et al. (2014). C9orf72 repeat expansions cause neurodegeneration in *Drosophila* through arginine-rich proteins. *Science* 345, 1192–1194.
- Molliex, A., Temirov, J., Lee, J., Coughlin, M., Kanagaraj, A.P., Kim, H.J., Mit-tag, T., and Taylor, J.P. (2015). Phase separation by low complexity domains promotes stress granule assembly and drives pathological fibrillization. *Cell* 163, 123–133.
- Mori, K., Weng, S.M., Arzberger, T., May, S., Rentzsch, K., Kremmer, E., Schmid, B., Kretschmar, H.A., Cruts, M., Van Broeckhoven, C., et al. (2013). The C9orf72 GGGGCC repeat is translated into aggregating dipep-tide-repeat proteins in FTL/ALS. *Science* 339, 1335–1338.
- Mücke, N., Wedig, T., Bürer, A., Marekov, L.N., Steinert, P.M., Langowski, J., Aebi, U., and Herrmann, H. (2004). Molecular and biophysical characteriza-tion of assembly-starter units of human vimentin. *J. Mol. Biol.* 340, 97–114.
- Naldini, L., Blömer, U., Gally, P., Ory, D., Mulligan, R., Gage, F.H., Verma, I.M., and Trono, D. (1996). In vivo gene delivery and stable transduction of nondividing cells by a lentiviral vector. *Science* 272, 263–267.
- Ogrodnik, M., Salmonowicz, H., Brown, R., Turkowska, J., Średniawa, W., Pattabiraman, S., Amen, T., Abraham, A.C., Eichler, N., Lyakhovetsky, R., and Kaganovich, D. (2014). Dynamic JUNQ inclusion bodies are asymmetri-cally inherited in mammalian cell lines through the asymmetric partitioning of vimentin. *Proc. Natl. Acad. Sci. USA* 111, 8049–8054.
- Patel, S.S., Belmont, B.J., Sante, J.M., and Rexach, M.F. (2007). Natively unfolded nucleoporins gate protein diffusion across the nuclear pore complex. *Cell* 129, 83–96.
- Patel, A., Lee, H.O., Jawerth, L., Maharana, S., Jahnel, M., Hein, M.Y., Stoynov, S., Mahamid, J., Saha, S., Franzmann, T.M., et al. (2015). A Liquid-to-Solid

- Phase Transition of the ALS Protein FUS Accelerated by Disease Mutation. *Cell* **162**, 1066–1077.
- Perez-Olle, R., Lopez-Toledano, M.A., and Liem, R.K. (2004). The G336S variant in the human neurofilament-M gene does not affect its assembly or distribution: importance of the functional analysis of neurofilament variants. *J. Neuropathol. Exp. Neurol.* **63**, 759–774.
- Pondel, M.D., and King, M.L. (1988). Localized maternal mRNA related to transforming growth factor beta mRNA is concentrated in a cyokeratin-enriched fraction from *Xenopus* oocytes. *Proc. Natl. Acad. Sci. USA* **85**, 7612–7616.
- Renton, A.E., Majounie, E., Waite, A., Simón-Sánchez, J., Rollinson, S., Gibbs, J.R., Schymick, J.C., Laaksovirta, H., van Swieten, J.C., Myllykangas, L., et al.; ITALSGEN Consortium (2011). A hexanucleotide repeat expansion in C9ORF72 is the cause of chromosome 9p21-linked ALS-FTD. *Neuron* **72**, 257–268.
- Schnapp, B.J., and Reese, T.S. (1982). Cytoplasmic structure in rapid-frozen axons. *J. Cell Biol.* **94**, 667–669.
- Schneider, C.A., Rasband, W.S., and Eliceiri, K.W. (2012). NIH Image to ImageJ: 25 years of image analysis. *Nat. Methods* **9**, 671–675.
- Shi, Y., Pellarin, R., Fridy, P.C., Fernandez-Martinez, J., Thompson, M.K., Li, Y., Wang, Q.J., Sali, A., Rout, M.P., and Chait, B.T. (2015). A strategy for dissecting the architectures of native macromolecular assemblies. *Nat. Methods* **12**, 1135–1138.
- Shin, J.S., Chung, K.W., Cho, S.Y., Yun, J., Hwang, S.J., Kang, S.H., Cho, E.M., Kim, S.M., and Choi, B.O. (2008). NEFL Pro22Arg mutation in Charcot-Marie-Tooth disease type 1. *J. Hum. Genet.* **53**, 936–940.
- Sokolova, A.V., Kreplak, L., Wedig, T., Mücke, N., Svergun, D.I., Herrmann, H., Aebi, U., and Strelkov, S.V. (2006). Monitoring intermediate filament assembly by small-angle x-ray scattering reveals the molecular architecture of assembly intermediates. *Proc. Natl. Acad. Sci. USA* **103**, 16206–16211.
- Taylor, M.S., LaCava, J., Mita, P., Molloy, K.R., Huang, C.R., Li, D., Adney, E.M., Jiang, H., Burns, K.H., Chait, B.T., et al. (2013). Affinity proteomics reveals human host factors implicated in discrete stages of LINE-1 retrotransposition. *Cell* **155**, 1034–1048.
- Tetko, I.V., Gasteiger, J., Todeschini, R., Mauri, A., Livingstone, D., Ertl, P., Palyulin, V.A., Radchenko, E.V., Zefirov, N.S., Makarenko, A.S., et al. (2005). Virtual computational chemistry laboratory—design and description. *J. Comput. Aided Mol. Des.* **19**, 453–463.
- Updike, D.L., Hachey, S.J., Kreher, J., and Strome, S. (2011). P granules extend the nuclear pore complex environment in the *C. elegans* germ line. *J. Cell Biol.* **192**, 939–948.
- US EPA. (2016). Estimation Programs Interface Suite for Microsoft Windows, v 4.11. United States Environmental Protection Agency, Washington, DC, USA.
- van Blitterswijk, M., Gendron, T.F., Baker, M.C., DeJesus-Hernandez, M., Finch, N.A., Brown, P.H., Daugherty, L.M., Murray, M.E., Heckman, M.G., Jiang, J., et al. (2015). Novel clinical associations with specific C9ORF72 transcripts in patients with repeat expansions in C9ORF72. *Acta Neuropathol.* **130**, 863–876.
- Vieira, N.M., Naslavsky, M.S., Licinio, L., Kok, F., Schlesinger, D., Vainzof, M., Sanchez, N., Kitajima, J.P., Gal, L., Cavaçana, N., et al. (2014). A defect in the RNA-processing protein HNRPD causes limb-girdle muscular dystrophy 1G (LGMD1G). *Hum. Mol. Genet.* **23**, 4103–4110.
- Wen, X., Tan, W., Westergard, T., Krishnamurthy, K., Markandaiah, S.S., Shi, Y., Lin, S., Shneider, N.A., Monaghan, J., Pandey, U.B., et al. (2014). Antisense proline-arginine RAN dipeptides linked to C9ORF72-ALS/FTD form toxic nuclear aggregates that initiate in vitro and in vivo neuronal death. *Neuron* **84**, 1213–1225.
- Wootton, J.C. (1994). Non-globular domains in protein sequences: automated segmentation using complexity measures. *Comput. Chem.* **18**, 269–285.
- Wu, H., and Fuxreiter, M. (2016). The Structure and Dynamics of Higher-Order Assemblies: Amyloids, Signalosomes, and Granules. *Cell* **165**, 1055–1066.
- Xiang, S., Kato, M., Wu, L.C., Lin, Y., Ding, M., Zhang, Y., Yu, Y., and McKnight, S.L. (2015). The LC Domain of hnRNP A2 Adopts Similar Conformations in Hydrogel Polymers, Liquid-like Droplets, and Nuclei. *Cell* **163**, 829–839.
- Zu, T., Liu, Y., Bañez-Coronel, M., Reid, T., Pletnikova, O., Lewis, J., Miller, T.M., Harms, M.B., Falchook, A.E., Subramony, S.H., et al. (2013). RAN proteins and RNA foci from antisense transcripts in C9ORF72 ALS and frontotemporal dementia. *Proc. Natl. Acad. Sci. USA* **110**, E4968–E4977.

## STAR★METHODS

## KEY RESOURCES TABLE

REAGENT or RESOURCE	SOURCE	IDENTIFIER
<b>Antibodies</b>		
Mouse monoclonal anti-Flag	Sigma-Aldrich	Cat#F3165; RRID: AB_259529
Rabbit polyclonal anti-HA	Santa Cruz	Cat#SC-805; RRID: AB_631618
Goat polyclonal anti-TIA1	Santa Cruz	Cat#SC-1751; RRID: AB_2201433
Mouse polyclonal anti-coilin	Abcam	Cat#AB-167253
Rabbit polyclonal anti-SC35	Santa Cruz	Cat# SC-28720; RRID: AB_2185049
Rabbit monoclonal anti-vimentin	Cell-signaling	Cat#5741S
Mouse monoclonal anti-keratin	Cell-signaling	Cat#4545S
Mouse monoclonal anti-tubulin	Sigma-Aldrich	Cat#T5168; RRID:AB_477579
Goat-anti-rabbit IgG-HRP conjugate	Bio-rad	Cat#170-6515; RRID: AB_11125142
Goat-anti-mouse IgG-HRP conjugate	Bio-rad	Cat#172-1011; RRID: AB_11125936
AlexaFluor 488 conjugated donkey anti-goat IgG	Thermo Fisher Scientific	Ref# A11055; RRID: AB_142672
AlexaFluor 488 conjugated donkey anti-mouse IgG	Thermo Fisher Scientific	Ref# A21202; RRID: AB_2535788
Anti-flag magnetic beads	Conjugated using anti-Flag antibody (Sigma) and Dynabeads (Invitrogen)	Ref#14301
Anti-HA magnetic beads	Thermo Fisher Scientific	Prod#88837
<b>Chemicals, Peptides, and Recombinant Proteins</b>		
Ni-NTA agarose resin	QIAGEN	Cat No./ID: 30230
PR <sub>20</sub> HA	UT Southwestern Protein Chemistry Core	N/A
PR <sub>20</sub> BAH	UT Southwestern Protein Chemistry Core	N/A
Tris[(1-benzyl-1H-1,2,3-triazol-4-yl)methyl] amine	TClchemicals	Cat#T2993
CuSO <sub>4</sub>	Sigma-Aldrich	Cat#451657
Tris(2-carboxyethyl) phosphine hydrochloride	TClchemicals	Cat#T1656
Diazo Biotin-Azide	Click Chemistry Tools	Cat#1041
1,6-Hexandiol	Sigma-Aldrich	Cat#240117
2,5-Hexandiol	Sigma-Aldrich	Cat#H11904
1,5-Pentandiol	Sigma-Aldrich	Cat#76892
1,4-Butandiol	Sigma-Aldrich	Cat#493732
A $\beta$ -40 fibrils	Dr. Robert Tycko	N/A
Sup35NM	Dr. Randal Halfmann	N/A
FITC-phalloidin	Sigma-Aldrich	Cat#P5282
tubulin	Cytoskeleton Inc.	Cat#T240-A
actin	Cytoskeleton Inc.	Cat#AKL95-B
Guanosine-5'-[( $\alpha$ , $\beta$ )-methylene]triphosphate	Jena Bioscience	Cat#NU-405
<b>Critical Commercial Assays</b>		
Pierce BCA protein assay kit	Thermo Scientific	Cat#23227
<b>Recombinant DNA</b>		
pCW-3xFlag-PR <sub>100</sub> -HA	This paper	N/A
pMD2.g	Addgene	12259
pSPAX2	Addgene	12260
pHis-Parallel-mCherry-FUS N214	<a href="#">Kato et al., 2012</a>	N/A
pHis-Parallel-FUS N214	<a href="#">Kato et al., 2012</a>	N/A
pHis-Parallel-GFP-FUS N214	<a href="#">Kato et al., 2012</a>	N/A
MBP-PTB-hnRNPA2 LC	<a href="#">Xiang et al., 2015</a>	N/A

(Continued on next page)

**Continued**

REAGENT or RESOURCE	SOURCE	IDENTIFIER
pHis-Parallel-GFP-hnRNPA2 LC	<a href="#">Kato et al., 2012</a>	N/A
pHis-Parallel-GFP-hnRNPA1 full-length	This paper	N/A
pHis-Parallel-GFP-hnRNPA1 LC	<a href="#">Kato et al., 2012</a>	N/A
pHis-Parallel-GFP-hnRNPA1 $\Delta$ LC	This paper	N/A
pHis-Parallel-GFP-hnRNPDLC	This paper	N/A
pHis-Parallel-mCherry-Neurofilament Light/Medium/Heavy Head	This paper	N/A
pHis-Parallel-mCherry-Vimentin Head	This paper	N/A
pHis-Parallel-GFP-Peripherin Head	This paper	N/A
pET28-Vimentin Full length	This paper	N/A
pET28-Vimentin Tailless	This paper	N/A
pET28-Vimentin Headless	This paper	N/A
pHis-GFP-PR <sub>20</sub>	<a href="#">Kwon et al., 2014</a>	N/A
pHis-GFP	<a href="#">Kato et al., 2012</a>	N/A
<b>Software and Algorithms</b>		
Prism 6	Graphpad Software	<a href="http://www.graphpad.com/scientific-software/prism/">http://www.graphpad.com/scientific-software/prism/</a>
SEG Prediction of low complexity regions	IMP Bioinformatics Group	<a href="http://www.biology.wustl.edu/gcg/seg.html">www.biology.wustl.edu/gcg/seg.html</a>
VCCLab		<a href="http://www.vcclab.org">www.vcclab.org</a>
ACD/Labs		<a href="http://www.acdlabs.com">www.acdlabs.com</a>
EPISuite		<a href="http://www.epa.gov/tsca-screening-tools/epi-suite-estimation-program-interface">www.epa.gov/tsca-screening-tools/epi-suite-estimation-program-interface</a>
ChemAxon		<a href="http://www.chemaxon.com">www.chemaxon.com</a>
<b>Experimental Models: Cell Lines</b>		
U2OS	ATCC	HTB-96
HeLa	ATCC	CCL-2
HEK293T Lenti-X	Clontech	Cat# 632180
U2OS PR <sub>100</sub> -3xFlag stable cell line	This paper	N/A

**CONTACT FOR REAGENT AND RESOURCE SHARING**

Steven McKnight ([steven.mcknight@utsouthwestern.edu](mailto:steven.mcknight@utsouthwestern.edu))

**METHOD DETAILS****Synthesis of PR<sub>20</sub>HA and PR<sub>20</sub>BAH Peptide**

Peptide containing 20 repeats of PR with an HA epitope tag at the C terminus (PR<sub>20</sub>HA) was synthesized from the Protein Chemistry Core at UT Southwestern Medical Center, as described previously ([Kwon et al., 2014](#)). To make a photo crosslinkable PR<sub>20</sub>BAH peptide, benzophenone was conjugated to the peptidyl-resin using HATU activation. Deprotection and cleavage of the peptide was achieved using 95% TFA containing thiol scavengers. The cleavage reaction was performed at room temperature for 2.5 hr and the cleaved peptide was precipitated in cold diethyl ether, centrifuged and the pellet washed several times with fresh diethyl ether. Purification of the peptide was achieved using a C18 Vydac (Hisperia CA) semi-preparative reversed-phase high-pressure liquid chromatography column (250 × 10 mm) on a Waters 600 HPLC system. Fractions were analyzed on a Vydac C18 analytical column (150 × 4.6 mm). Separations were achieved using linear gradients of 0 to 100% buffer B for 180 or 30 min, at a flow rate of 3 or 1 ml/min, respectively. Buffer A was water/0.045% TFA and buffer B was acetonitrile/0.036% TFA. Detection at 220 nm. The identity of the peptide was confirmed using an Agilent Q-TOF ESI-MS, model 6500 series.

**Live-Cell Crosslinking Using PR<sub>20</sub>BAH Probe**

HeLa cells were incubated with 10  $\mu$ M of PR<sub>20</sub>BAH in culture medium for 3 hr at 37°C, followed by UV (306 nm) crosslinking using the Stratalinker 2400 (Stratagene). Cells were harvested, washed with PBS and resuspended in lysis buffer (Tris-HCl [pH7.5], 200 mM NaCl, 20 mM  $\beta$ -mercaptoethanol, 0.5 mM EDTA, and Sigmafast protease inhibitor [Sigma-Aldrich, St. Louis, MO]). After sonication,

cell debris were removed by centrifugation at 13,400 rpm. To perform the copper-catalyzed click reaction, 100  $\mu$ M Tris [(1-benzyl-1H-1,2,3-triazol-4-yl) methyl] amine, 2 mM CuSO<sub>4</sub>, 1 mM Tris (2-carboxyethyl) phosphine, and 100  $\mu$ M Diazo Biotin-Azide (Click Chemistry Tools 1041) were added to cell lysates and the mixture was incubated for 1 hr at room temperature with constant agitation. Proteins were then precipitated by adding four volumes of cold acetone and re-solubilized for overnight in PBS containing 4% SDS and 7 M urea. Lysates were cleared by filtration through 0.22  $\mu$ m filters. Streptavidin agarose resins (Thermo Fisher Scientific, Waltham, MA) were added to the re-solubilized protein and incubated for 1 hr with mild rotation at 25°C. After three washes with 4% SDS in PBS, bound proteins were eluted in Laemmli sample buffer by boiling at 95°C for 10 min. Eluted proteins were resolved via SDS-PAGE, and the gel was stained with the Instant Blue (Expedeon, San Diego, CA). The resolved proteins were excised and sent for mass spectrometric analysis.

To attach fluorescent tag to PR<sub>20</sub>BAH-crosslinked proteins, a similar click reaction was performed as described above. For this reaction, 100  $\mu$ M Alexa 532 azide was added instead of Diazo Biotin-Azide. After 1 hr of reaction, samples were mixed with Laemmli sample buffer and the proteins were resolved by SDS-PAGE. Fluorescence was imaged using a Typhoon scanner (GE Healthcare Bio-Sciences, Pittsburgh, PA).

### Construction of Flag-PR<sub>100</sub>-HA Stable Cell Line

DNA fragment encoding 100 repeats of PR, with 3xFlag at the N terminus and HA epitope tag at the C terminus, was synthesized by Genewiz (South Plainfield, NJ) and subcloned into the pCW57.1 doxycycline-inducible lentiviral plasmid. To generate lentiviral particles, pCW-3xFlag-PR<sub>100</sub>-HA plasmid was co-transfected with pMD2.g (Addgene 12259) and pSPAX2 (Addgene 12260) into 293T cells (Naldini et al., 1996). To generate an inducible stable cell lines for 3xFlag:PR<sub>100</sub>, U2OS cells were infected with lentivirus collected from transfected 293T cells in the presence of 8  $\mu$ g/ml polybrene. Infected cells were selected with 2  $\mu$ g/ml puromycin for 3 days.

### Cryogenic Extraction and Affinity Purification of PR<sub>100</sub>

After induction of Flag-PR<sub>100</sub>-HA with doxycycline for 48 hr, cells were detached, washed in PBS and then collected in liquid nitrogen. Cells were then ground using a cryomill (Retsch, Newtown, PA). In brief, frozen cells were placed in a grinding chamber with stainless steel balls, all pre-cooled by liquid nitrogen. Cryomill grinding was performed for three cycles of 1 min, 30 Hz. The grinded cell powder was stored at -80°C. Anti-Flag antibody (Sigma-Aldrich, St. Louis, MO) was coupled to Dynabeads M-270 epoxy (Thermo Fisher Scientific, Waltham, MA) at the ratio of 10  $\mu$ g of antibody/mg beads. For immunoprecipitation, 100  $\mu$ L of IP buffer (20 mM HEPES [pH 7.4], 110 mM potassium acetate, 2 mM MgCl<sub>2</sub>, 150 mM NaCl, 0.05% NP-40) was added to 100 mg of cell powder. After brief sonication and a quick spin at 13,400 rpm at 4°C, the supernatant was collected. 5  $\mu$ L of anti-Flag Dynabeads were incubated with cell lysate for 1 min and the immune complex was washed with IP buffer three times. Bound proteins were eluted with 1 mg/ml 3xFlag peptide, followed by SDS-PAGE.

### Proteomic Analysis and Computation Analysis of LC Sequences

The Commassie-stained gel was sent to the Taplin Biological Mass Spectrometry Facility at Harvard Medical School for proteomic analysis. LC sequences were identified using the SEG algorithm (Wootton, 1994), with window = 25, locut = 2.2 and hicut = 2.5. Entries containing continuous LC sequences no shorter than 50 amino acids were considered LC containing proteins. P values were calculated assuming hypergeometric distribution using web server <https://www.geneprof.org/GeneProf/tools/hypergeometric.jsp>.

### Immunoprecipitation of hnRNPA1 Domain Constructs

Full-length (residue 2-320),  $\Delta$ LCS (2-185) or  $\Delta$ RRM (186-320) of human hnRNPA1 were subcloned into pHis-parallel-GFP vector and transformed into BL21 (DE3) competent cells. Expression of hnRNPA1 proteins was induced by 1 mM IPTG at 25°C for 3 hr. Cells were harvested and frozen in liquid nitrogen, followed by five cycles of 1 min cryomill grinding at 30 Hz. Cell powder was homogenized in a lysis buffer (20 mM Tris-HCl pH 7.5, 500 mM NaCl, 20 mM BME, 0.5 mM EDTA, 0.1 mM PMSF supplemented with Sigmafast protease inhibitor) by sonication for 30 s. Cell debris was removed by 20 min of ultracentrifugation at 35,000 rpm. All three proteins were first purified through a Ni-NTA column. hnRNPA1  $\Delta$ LCS was then subject to size-exclusion chromatography using a HiLoad 26/60 Superdex 200 column (GE Healthcare, Marlborough, MA). The hnRNPA1 full-length and  $\Delta$ RRM proteins were further purified by a Phenyl Superose FPLC column (GE Healthcare, Marlborough, MA). Purified proteins were dialyzed with gelation buffer and concentrated to 20 mg/ml. For immunoprecipitation, proteins were diluted to 1 mg/ml in gelation buffer containing 0.05% NP-40, rotated for 1 hr at room temperature, and PR<sub>20</sub>HA peptide and anti-HA beads were added, followed by 30 min incubation. The beads were washed three times and eluted with glycine buffer (pH 2.6). Eluted proteins were subject to SDS-PAGE analysis. The amount of PR<sub>20</sub>HA was quantified by dot blot, using anti-HA antibody (Santa Cruz, Dallas, TX).

### Preparation of GFP- and mCherry-Fusion Proteins

GFP- or mCherry:FUS LC domain (residue 2-214) was prepared as described previously (Kato et al., 2012). DNA fragments encoding the head domains of human IF proteins (Neurofilament (NF) Heavy: residue 3-100, NF Medium: 2-104, NF Light: 2-100, Vimentin: 2-95, Peripherin: 2-99) were amplified by PCR using human cDNA as a template. The DNA fragments were inserted into the BamHI/XhoI sites of the pHis-parallel-GFP or pHis-parallel-mCherry plasmid (Kato et al., 2012). Pathogenic mutations in the hnRNP

LC domains (hnRNPA1: residue 186-320, hnRNPA2: 181-341, and hnRNPD: 323-420) were introduced by a quickchange method using wild-type GFP:hnRNP constructs as templates. Expression and purification of the wild-type and mutants of GFP:hnRNPs were carried out as described previously (Xiang et al., 2015).

All IF head domains were overexpressed in *E. Coli* BL21 (DE3) cells with 0.5 mM IPTG at 20°C for overnight. Harvested cells were lysed with 0.4 mg/mL lysozyme in a lysis buffer containing 50 mM Tris-HCl pH7.5, 500 mM NaCl, 20 mM  $\beta$ -mercaptoethanol (BME), 1% Triton X-100, 2 M guanidine hydrochloride (GdnHCl) and protease inhibitor cocktail (Sigma-Aldrich, USA) for 30 min on ice, and then sonicated for 2 min. The cell lysates were centrifuged at 35,000 rpm for 1 hr. The supernatants were mixed with 10 ml Ni-NTA resin (QIAGEN, USA) for 30 min at 4°C. The Ni-NTA resin was packed in a glass column and then washed with washing buffer (300 ml) containing 20 mM Tris-HCl pH7.5, 500 mM NaCl, 20 mM imidazole, 20 mM BME, 0.1 mM PMSF and 2 M GdnHCl. The resin was further washed with the washing buffer (50 ml) containing 2 M Urea instead of GdnHCl. Bound proteins were eluted from the resin with an elution buffer containing 20 mM Tris-HCl pH7.5, 500 mM NaCl, 250 mM imidazole, 20 mM BME, 0.1 mM PMSF and 2 M Urea. EDTA was added to the elution at a final concentration of 0.5 mM. The purified proteins were concentrated with Amicon Ultra centrifugal filters (Millipore, USA). Glycerol was added to the GFP fusion proteins at a final concentration of 50%. The protein solutions were kept at –20°C. The mCherry fusion proteins were kept at –80°C without glycerol. Protein purity was checked by SDS-PAGE, and concentrations were determined by absorbance at UV<sub>280</sub>.

### Preparation and Characterization of Fibers/Hydrogels

Fibers or hydrogel droplets of mCherry:FUS LC domain and GFP:hnRNPA2 LC domains were prepared as described previously (Kato et al., 2012; Xiang et al., 2015). Fibers or hydrogel droplets of the head domains of intermediate filament proteins were prepared as follows: the mCherry:head domains were dialyzed in a gelation buffer containing 20 mM Tris-HCl pH 7.5, 50 mM NaCl, 20 mM BME, 0.5 mM EDTA and 0.1 mM PMSF for overnight at room temperature (RT). Dialyzed proteins were sonicated briefly (1 s x 3 times), centrifuged to remove precipitates, and then concentrated to approximately 50-100 mg/ml. Small droplets (0.5  $\mu$ l) of the protein solution were made in glass-bottomed 35-mm culture dishes (MatTek, USA) and left at RT for 2-3 days.

To inspect fiber formation, the concentrated protein solution was diluted 10-fold with gelation buffer and deposited on a surface of a TEM grid (CF-400-Cu from Electron Microscopy Sciences, USA). The surface of the grid was washed three times with 10  $\mu$ L of distilled water. The grid was subsequently stained for a few seconds with a 5  $\mu$ L drop of 2% uranyl acetate. After the uranylacetate solution was blotted, the grid was dried in air. TEM images were obtained with a JEOL 1200EX electron microscope at 120 kV.

For fiber X-ray diffraction, the hydrogels or precipitated fiber materials were resuspended in 0.2 ml milli-Q water and dialyzed in 1 L milli-Q water for 12 hr twice. The dialyzed samples were lyophilized for overnight and then exposed to an X-ray beam to obtain cross- $\beta$  diffraction as described previously (Kato et al., 2012).

The stability of cross- $\beta$  fibers of IF head domains and pathogenic mutants of hnRNPs were examined by SDD-AGE. Fiber solutions were diluted in gelation buffer and sonicated briefly to make fibers short. The short fibers were incubated in gelation buffer containing different concentrations of SDS (0–2%) at 37°C for 10 min. As a control, amyloid fibers of yeast Sup35NM protein were treated in the same way. The reaction mixtures were loaded on 1.5% agarose gel to separate fibers and monomers. The agarose gel was scanned by a fluorescent imager (Typhoon 9200, GE) to visualize GFP or mCherry-fusion proteins. Subsequently, proteins were transferred onto a cellulose membrane and analyzed by western blotting with a His-tag antibody to visualize Sup35NM bands as described previously (Kato et al., 2012).

### Melting of Fibers/Hydrogels by Aliphatic Alcohols

Hydrogel droplets of mCherry:FUS LC domain were exposed to 2 ml 15% of different aliphatic alcohols at 37°C, and mCherry signals of the droplets were scanned by a confocal fluorescent microscope at indicated time points.

Fiber melting by aliphatic alcohols was monitored by turbidity measurements (absorbance at a 395 nm wavelength). Fibers of mCherry:FUS LC domain or mCherry:IF head domains were diluted in gelation buffer to obtain a final protein concentration of 100  $\mu$ M (monomer based). A brief 1 s sonication was applied to break down longer fibers. Sonicated fibers were further diluted to obtain initial OD<sub>395</sub> of 0.06–0.1. The fiber solution was incubated at 37°C in the presence of various concentrations of 1,6-HD or 15% of different alcohols, and the OD<sub>395</sub> was measured at indicated time points. For the melting of A2 LC domain fibers, samples with indicated concentrations of aliphatic alcohols were dispensed (100  $\mu$ l) onto a 384-well plate (Greiner Bio-One) and incubated at 37°C. The absorbance at 395nm (turbidity) was monitored as a function of time by the Bio-Tek Cytation 5 imaging reader.

### Melting of Sub-cellular Structures by Aliphatic Alcohols

To test the effect of aliphatic alcohols on stress granules, HeLa cells were treated with 0.5 mM sodium arsenite for 1 hr, exposed to 6% aliphatic alcohols for 5 min, and fixed with 4% PFA for 15 min. The fixed cells were incubated with 1:300 goat anti-TIA1 (Santa Cruz, Dallas, TX) overnight at 4°C, and developed with 1:300 AlexaFluor 488 conjugated donkey anti-goat (Thermo Fisher Scientific, Waltham, MA) for 1 hr at room temperature. To study other subcellular granules, non-treated HeLa cells were exposed to 6% - 8% level of aliphatic alcohols, fixed with 4% PFA, incubated with mouse anti-coilin (Pdelta, 1:1,000, Abcam, Cambridge, MA) or mouse anti-SC35 (1:500, Abcam, Cambridge, MA), respectively, at 4°C overnight, and stained with AlexaFluor 488 conjugated secondary antibody against mouse IgG (1:500, Thermo Fisher Scientific, Waltham, MA).

To study the effects of aliphatic alcohols on cytoskeleton filaments, HeLa cells were treated with 8% aliphatic alcohols for five minutes at room temperature and fixed. Cells fixed by 4% PFA were stained with 1.5  $\mu\text{g/ml}$  FITC-labeled phalloidin dissolved in PBST (PBS added with 0.2% Triton X-100) at 4°C overnight to visualize F-actin, or incubated with mouse anti-tubulin (1:1,500, Sigma-Aldrich, St. Louis, MO) at 4°C overnight, and developed with AlexaFluor 488 conjugated secondary antibody against mouse IgG (1:500, Thermo Fisher Scientific, Waltham, MA). Cells fixed with ice-cold methanol were incubated with pan-keratin mouse antibody (C11, 1:300, Cell Signaling Technologies, Danvers, MA) or rabbit monoclonal antibody against vimentin (D21H3, 1:100, Cell Signaling Technologies, Danvers, MA) at 4°C overnight, and stained with AlexaFluor 488 conjugated secondary antibodies (1:500, Thermo Fisher Scientific, Waltham, MA). Images showing the effect of aliphatic alcohols on vimentin filaments were taken with Leica TCS SP5 confocal microscope. All other images were taken using a Delta Vision Elite microscope (GE Healthcare Bio-Sciences Pittsburgh, PA) using the FITC channel.

### Melting of PTB:hnRNPA2 LC Liquid-Like Droplets by Aliphatic Alcohols

Liquid-like droplets of PTB:hnRNPA2 LC were prepared as described (Xiang et al., 2015). Briefly, triple fusion protein MBP:PTB:hnRNPA2 LC was mixed with RNA substrate and TEV protease, and incubated for 20 min at room temperature. The liquid-like droplets were exposed to 0%–4% level of aliphatic alcohols, incubated at room temperature for one minute and measured by light scattering at 395 nm. His<sub>6</sub>-tagged FUS LCS was concentrated to 2.5 mM in urea buffer (25 mM HEPES pH 7.4, 2 M urea, 5 mM BME). The protein stock was diluted 40 times in droplet buffer (10 mM HEPES pH 7.4, 100 mM KCl, 2% glycerol) supplemented with aliphatic alcohols to indicated concentration. The formation of liquid-like droplets was measured by light scattering at 395 nm.

### Immunoprecipitation of hnRNPA2 LCS in the Presence of Aliphatic Alcohols

His-3xFlag tagged recombinant proteins of wild-type, D290V or F291S hnRNPA2 LCS (181-341 aa) were purified as described previously (Kato et al., 2012). For immunoprecipitation, the proteins were diluted to 0.05 mg/ml in gelation buffer containing 0.05% NP-40 supplemented with indicated concentrations of aliphatic alcohol and then rotated for 1 hr at RT. After addition of both PR<sub>20</sub>HA peptide and anti-HA beads, samples were further incubated for another 30 min. Anti-HA beads were washed three times with PBS and bound proteins were eluted by glycine buffer (pH 2.6). Eluted proteins were subjected to western-blot analysis against anti-Flag antibody (Sigma, St. Louis, MO).

### Assembly of Recombinant Vimentin Intermediate Filaments

Recombinant proteins of human vimentin [full length (2-466 AA),  $\Delta$ head (82-466 AA),  $\Delta$ tail (2-411 AA)] were expressed and purified. Bacterial pellet was solubilized in lysis buffer (50 mM Tris-HCl, pH7.5, 500 mM NaCl, 20 mM BME, 1% Triton X-100 with protease inhibitor cocktail), and inclusion bodies were isolated by centrifugation. Inclusion bodies were solubilized with urea lysis buffer (8 M urea, 50 mM Tris-HCl, pH7.5, 20 mM BME), and the solubilized protein samples were further purified by Q-Sepharose column chromatography and gel-filtration. Purified vimentins were kept in 8 M urea at 2-6 mg/mL and stored at –80°C. For intermediate filament assembly, vimentin was dialyzed into 2 mM sodium phosphate buffer (pH7.5) containing 1 mM DTT. Dialysis was performed at room temperature in a stepwise manner (8, 4, 2, and 0 M urea) for two hour intervals and continued at 4°C with 0 M urea for over night. The protein sample was further dialyzed into 2 mM sodium phosphate buffer without DTT for an additional hour. For starting assembly, the dialyzed protein solution at 0.2 mg/mL was mixed with an equal amount of 2x assembly buffer (200 mM KCl, 2 mM sodium phosphate buffer, pH7.5), and incubated at 37°C for 1 hr.

### Assembly of Actin and Tubulin Filaments

Actin protein (> 95% pure) from rabbit skeletal muscle (Cytoskeleton Inc, Denver, CO) was dissolved in buffer A (0.5 mM ATP, 0.2 mM CaCl<sub>2</sub>, 0.5 mM DTT, 0.02% NaN<sub>3</sub>, 2 mM Tris-HCl, titrated at 4°C to pH 8.0 with KOH). Actin filament assembly was initiated by adding 10% volume of 10xKMEI buffer (500 mM KCl, 10 mM MgCl<sub>2</sub>, 10 mM EGTA, 100 mM Imidazole HCl, pH 7.0) directly into the protein solution, and incubate at 37°C for 1 hr.

Tubulin protein (> 99% pure) from porcine brain (Cytoskeleton Inc, Denver, CO) was dissolved in BRB80 buffer (80 mM PIPES, 1 mM MgCl<sub>2</sub>, 1 mM EGTA, pH 6.8 with KOH) with 1 mM DTT and 1 mM guanosine-5'-[( $\alpha,\beta$ )-methylene]triphosphate (GMPCPP, non-hydrolyzable GTP analog) (Jena Bioscience, Germany) to obtain a concentration of 2 mg/mL on ice. The protein was assembled into microtubule by diluting the protein sample to 0.2 mg/mL with BRB80 buffer with 1 mM DTT. Assembly was carried out by incubating the sample at 37°C for 1 hr.

### Melting of Filaments by Aliphatic Alcohols

Preassembled filaments (vimentin intermediate filament, actin filament, tubulin filament) at 0.2 mg/mL were challenged by hexanediol melting at 2.5% by adding equal volume of 5% hexanediols in each assembly buffer conditions. The mixtures were incubated for indicated time at 37°C, and the reaction was stopped by adding equal amount of buffer containing 0.2% glutalaldehyde.

### GFP:PR<sub>20</sub> Binding to Cytoskeletal Filaments

Preassembled filaments (vimentin, actin and microtubules) at 1  $\mu\text{M}$  were mixed with 0.3  $\mu\text{M}$  of GFP, GFP:PR<sub>20</sub> or GFP:FUS and incubated for 1 min at RT. Reaction were stopped by adding an equal volume of buffer containing 0.2% glutalaldehyde. Samples were then examined by transmission electron microscopy.

### Hydrophobicity Analysis of Aliphatic Alcohols

Four independent methods were used to predict hydrophobicity of aliphatic alcohols: VCCLab (Tetko et al., 2005), ACD/Labs (ACD/Structure Elucidator, 2015), EPISuite (US EPA, 2016), ChemAxon (<http://www.chemaxon.com>).

### QUANTIFICATION AND STATISTICAL ANALYSIS

Fiber/liquid-droplet melting experiments shown in Figures 2B, 2D, 2E, 4A, 4B, 5B, S2, and S6 were carried out in multiple measurements. The number of the experimental replication was indicated by “n” in the respective figure legends. Statistical analysis of the PR<sub>20</sub>-bound proteins shown in Figure 1C is carried out with the web server <https://www.geneprof.org/GeneProf/tools/hypergeometric.jsp>, assuming hypergeometric distribution. Quantification of distances/sizes of the RP<sub>20</sub> knobs along vimentin filaments shown in Figure 6 was carried out with the program ImageJ (Schneider et al., 2012). The number of measurements is indicated by “n” in the figure legends. Curve fittings shown in Figures 6C and 6F were performed using the program Prism 6 (GraphPad Software, USA).

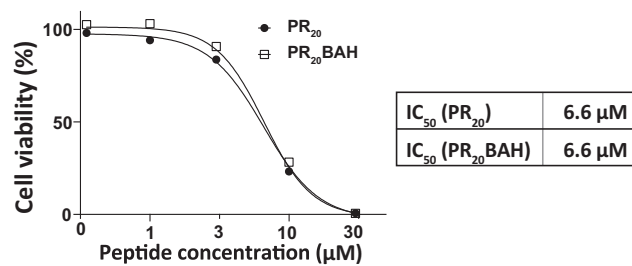


**Figure S1. Dose-Dependent Cell Death in Response to Either PR<sub>20</sub>HA or PR<sub>20</sub>BAH, Related to Figure 1**

U2OS cells were seeded in 96-well plates at the density of 3,000 cells/well. After overnight incubation, cells were treated with indicated concentration of PR<sub>20</sub>HA or PR<sub>20</sub>BAH. After 72 hr cells were lysed and viability was measured as described previously (Kwon et al., 2014).

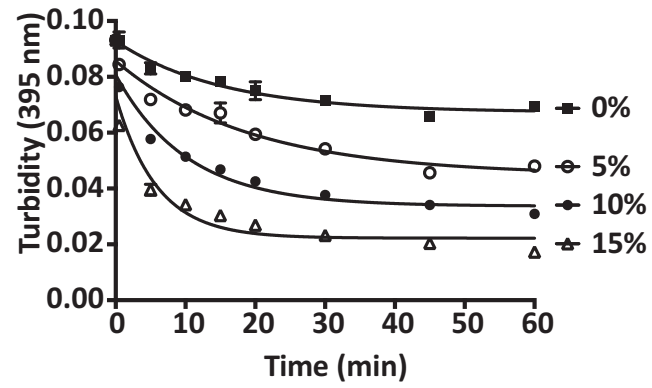
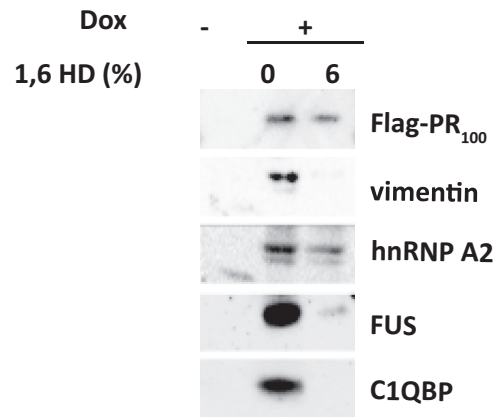
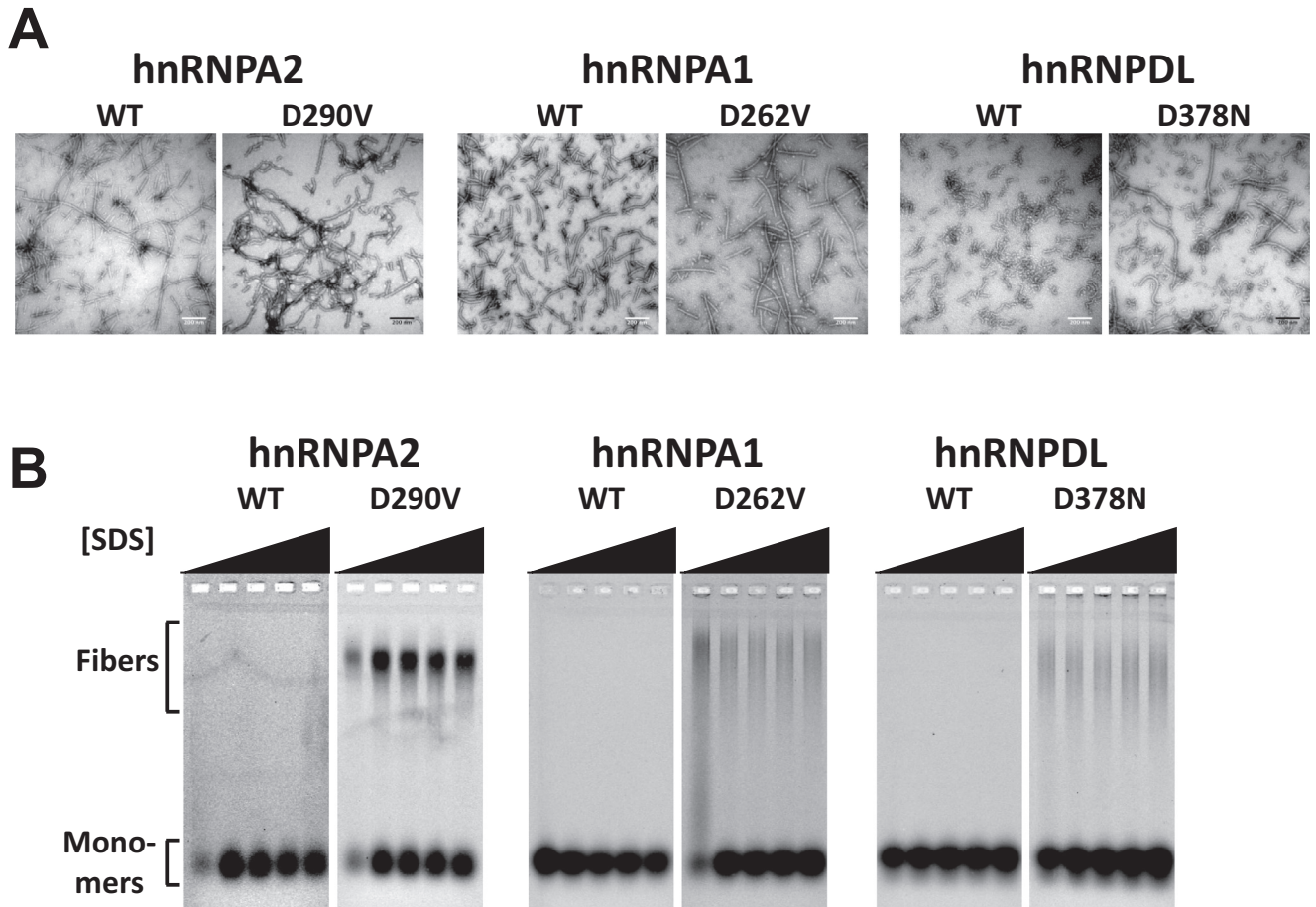


Figure S2. Melting of Pre-gelation mCherry:FUS Polymeric Fibers by Varying Concentrations of 1,6-Hexanediol, Related to [Figure 2](#)



**Figure S3. Effects of 1,6-Hexanediol on Co-immunoprecipitation of Cellular Proteins with Flag-Tagged PR<sub>100</sub>, Related to Figure 4**  
3xFlag:PR<sub>100</sub> expression was either induced with doxycycline (+) or without (-). The right two lanes show proteins co-precipitated with 3xFlag:PR<sub>100</sub> in the presence or absence of 6% 1,6-hexanediol.



**Figure S4. Disease Mutations Provoke Stabilized Polymers of hnRNP LC Domains, Related to Figure 4**

(A) Electron micrographs of polymeric fibers formed from GFP fused to the native LC domains of hnRNPA2, hnRNPA1 and hnRNPD L, or mutated variants bearing D-to-V (hnRNPA2), D-to-V (hnRNPA1) or D-to-N (hnRNPD L) mutations. Scale bar = 200 nm.

(B) SDD-AGE gel analysis of cross- $\beta$  fibers depicted in (A). Ascending triangles reflect incubation for 15 min at 37°C in buffer supplemented with SDS concentrations ranging from 0 (left lane of each gel) to 0.1%, 0.5%, 1% or 2%. GFP signals were detected on a fluorescence scanning imager.

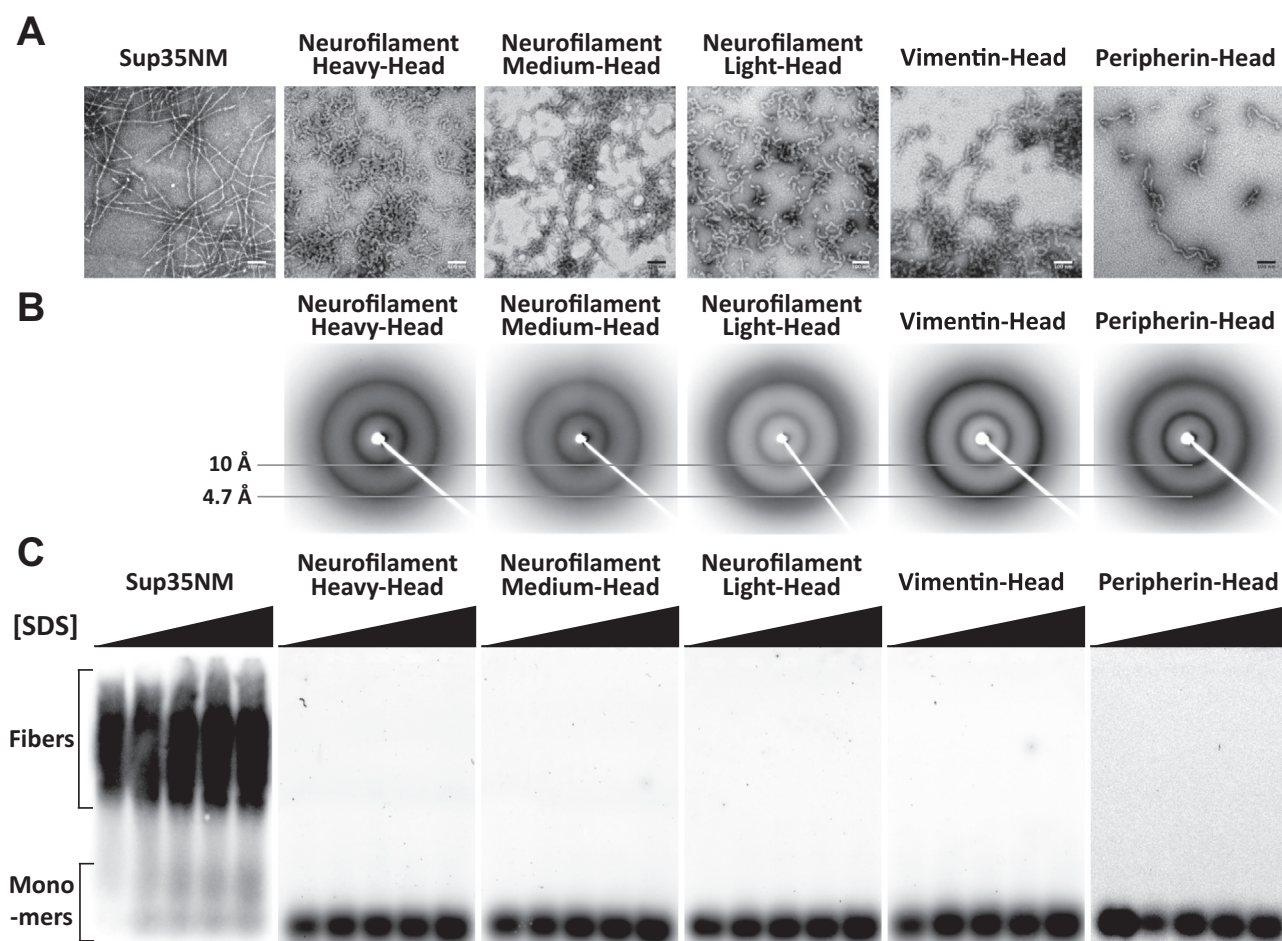


**Figure S5. Electron Microscope Images, X-Ray Diffraction Images and SDD-AGE Assays of mCherry Fusions to the Head Domains of Five Intermediate Filament Proteins, Related to Figure 5**

(A) Electron microscope images of polymeric forms of the yeast Sup35 protein and fusion proteins linking the low complexity head domains of the heavy, medium and light neurofilament isoforms and vimentin to mCherry, and the head domain of peripherin to GFP. Scale bar = 100 nm.

(B) X-ray diffraction patterns of hydrogels formed from the five indicated intermediate filament proteins.

(C) SDD-AGE assays of the stability of polymeric fibers made from the yeast Sup35 protein and the head domains of the five indicated intermediate filament proteins. Ascending SDS concentrations went from 0% to 0.1%, 0.5%, 1% or 2% (left to right).

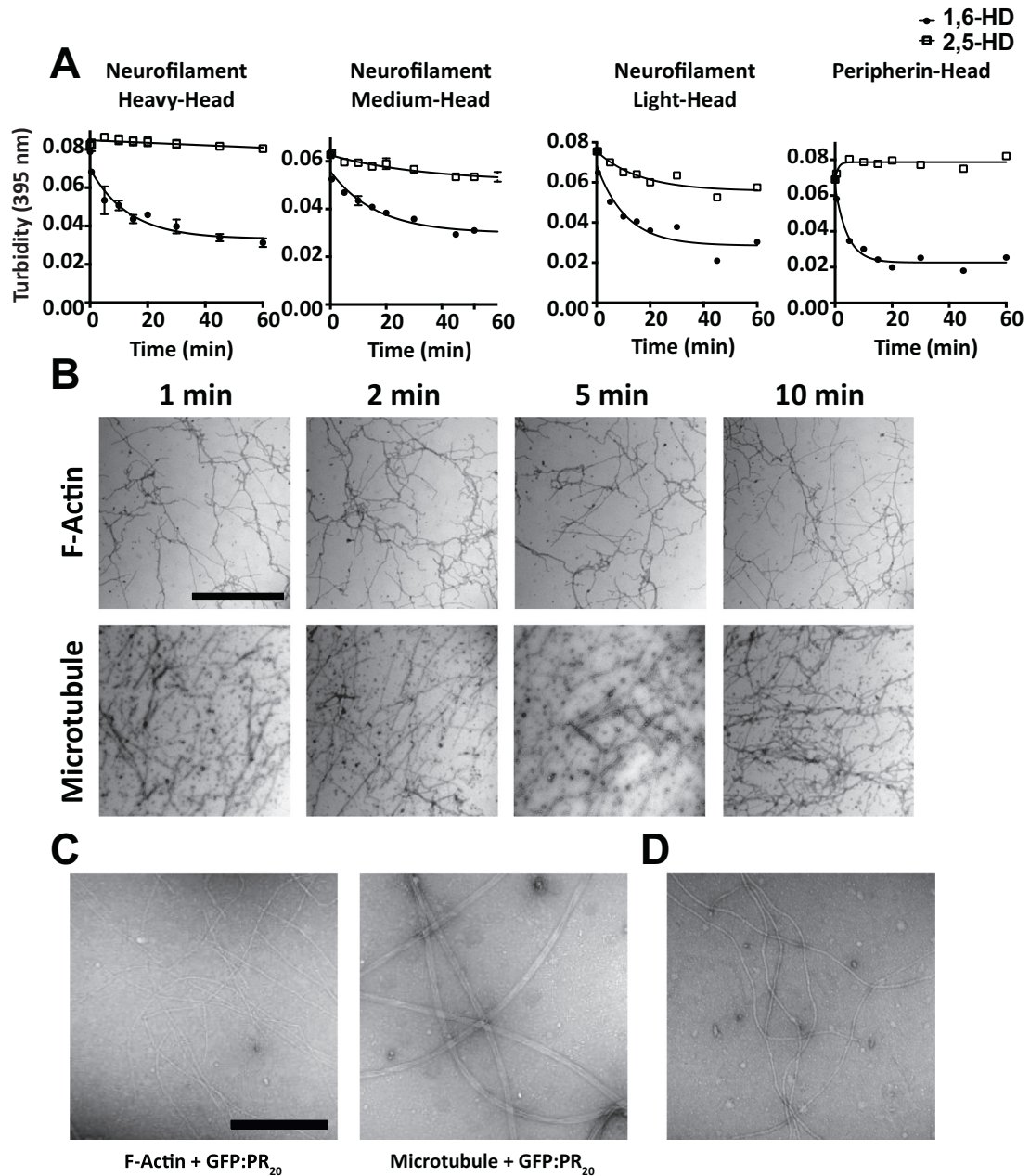


**Figure S6. Polymeric Fibers Formed from Low Complexity Domains Derived from Intermediate Filament Head Domains in Response to the Indicated Aliphatic Alcohols, and Electron Microscope Images of Intermediate Filaments, Related to Figures 5 and 6**

(A) Time-dependent melting of mCherry:NFH, mCherry:NFM, mCherry:NFL and mCherry:peripherin head domain polymers in suspension with 15% of indicated aliphatic alcohols as measured by light scattering at 395 nm ( $n = 2$  or  $3$ , data are presented as means  $\pm$  SD. Note that error bars for most of the data points are smaller than the symbols).

(B) Electron microscope images of F-actin filaments and microtubules exposed to 1,6-hexanediol for indicated times. Scale bar = 1  $\mu$ m.

(C) Electron microscope images of F-actin filaments and microtubules exposed to GFP:PR<sub>20</sub>. Scale bar = 500 nm.

(D) Electron microscope image of "tailless" vimentin intermediate filaments exposed to GFP:PR<sub>20</sub>.